The Molecular Design of Active Sites in Nanoporous Materials for Sustainable Catalysis

Stephanie Chapman[1], Matthew E. Potter [1] and Robert Raja [1,*]

[1] Department of Chemistry, University of Southampton, Highfield Campus, University Road, Southampton, SO17 1BJ, UK

* Correspondence: R.Raja@soton.ac.uk

Abstract:

At the forefront of global development, the chemical industry is being confronted by a growing demand for products and services, but also the need to provide these in a manner that is sustainable in the long-term. In facing this challenge, the industry is being revolutionized by advances in catalysis that allow chemical transformations to be performed in a more efficient and economical manner. To this end, molecular design, facilitated by detailed theoretical and empirical studies, has played a pivotal role in creating highly-active and selective heterogeneous catalysts. In this review, the industrially-relevant Beckmann rearrangement is presented as an exemplar of how judicious characterisation and *ab initio* experiments can be used to understand and optimise nanoporous materials for sustainable catalysis.

Keywords: Beckmann rearrangement, characterisation, structure-property correlations, zeotypes, acid sites.

1. Introduction

To meet the demands of an evolving global population, the chemical industry has expanded rapidly and, as a consequence, immense strain is being placed on both natural and synthetic resources. As a result of pressing environmental and economic concerns, the chemical industry has been driven towards more sustainable practices so that it can continue to meet the needs of the global populace.

The implementation of Green Chemistry is focal in the production of ubiquitous materials such as polymers and plastics, the precursors of which are predominantly derived from crude oil. Where processing chemical feedstocks to obtain higher-value products often involves many chemical transformations, catalysis has proven a widely-applicable and effective development. For example, many chemical processes invoke acid catalysis, and whilst mineral acids (such as hydrochloric and sulfuric acid) are accessible and cheap, their disposal, reuse and product purification are costly and detrimental to the environment. As a result, there has been an increasing shift towards the use of solid-acid catalysts that are more readily separated and recycled from fluid-phase reactions.

In this respect, the nylon industry is archetypal. As well as being the earliest synthetic polymers to be manufactured commercially, the polyamides (or nylons) have endured as some of the most industrially and economically important synthetic fibres in large-scale production.[1] Amongst the

40 aliphatic polyamides, nylon-6 and nylon-6,6 are notable due to their widespread application in
41 textiles and engineering resins; applications that exploit its characteristic elasticity, strength, and
42 physicochemical stability. In accord with consumer demand, the nylon-6,6/-6 industry has been
43 valued at $41.13 billion for 2025.[2]

44   Typically, nylons are produced by an irreversible condensation reaction between a diamine and
45 a dicarboxylic acid (Figure 1 (a)). Nylon-6, however, is formed by ring-opening polymerisation of the
46 ε-caprolactam monomer (Figure 1 (b)). As a result, nylon-6 can be depolymerized and recycled, with
47 > 99 % of the material recovered to make carpet yarn;[3] a lifecycle far more compatible with the
48 agenda for sustainable development.[4] In contrast, its non-recyclable analogue, nylon-6,6, (which is
49 formed by polymerisation condensation) can only be down-cycled for low-performance applications,
50 and ultimately terminates in landfill sites. Nylon-6 dominates the global resin market (~60 % total
51 consumption in 2016),[2] and given its extensive application in and textiles and engineering [5]
52 (requiring 6 million tonnes in 2015),[6] reducing the negative environmental impact of the material
53 lifecycle is hugely relevant. For this reason, there is significant interest, both in academia and
54 industry, in developing novel heterogeneous catalysts that offer greater sustainability in the
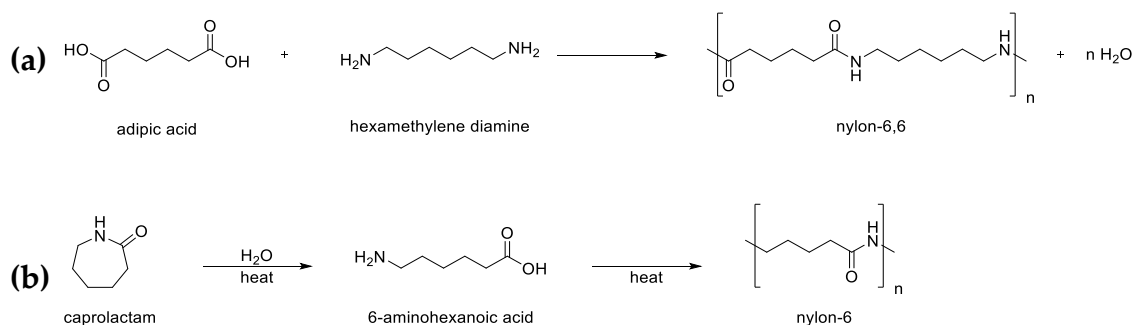55 production of nylon-6.

57 **Figure 1.** Scheme for the synthesis of the nylon-6,6 polymer through irreversible condensation
58   reaction between adipic acid and hexamethylene diamine (a), and the nylon-6 polymer by ring-
59   opening polymerisation of ε-caprolactam (b).

60   As well as being a fundamental precursor to nylon-6, ε-caprolactam is a high-value bulk
61 chemical in its own right, with a global output expected to exceed 4.6 megatonnes by 2018.[7]
62 Typically, ε-caprolactam is produced from cyclohexanone oxime in the acid-catalysed Beckmann
63 rearrangement. The Beckmann rearrangement is a classic, organic transformation in which an oxime
64 is converted into an amide through acid catalysis (Figure 2). Where a cyclic oxime substrate is used,
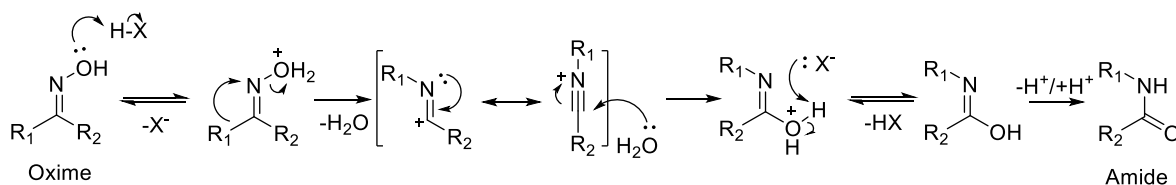65 a cyclic amide, or lactam, is formed.

67 **Figure 2.** The general mechanism of the Beckmann rearrangement, in which the transformation of an
68   oxime into an amide is facilitated by an acid catalyst (HX).

In the conventional, industrial route, this transformation is performed by a fuming sulphuric acid catalyst (oleum), in a multi-step process that generates disproportionate quantities of low-value ammonium sulphate by-product (Figure 3).[8] As this is both hazardous and inherently inefficient, conventional homogenous catalysts are being replaced by versatile solid-acid analogues. Besides their relatively facile recovery from fluid-phase reactions, heterogeneous catalysts also dispense with hazardous reagents and simultaneously alleviate the excessive amount of by-product generated by the traditional process.[9]
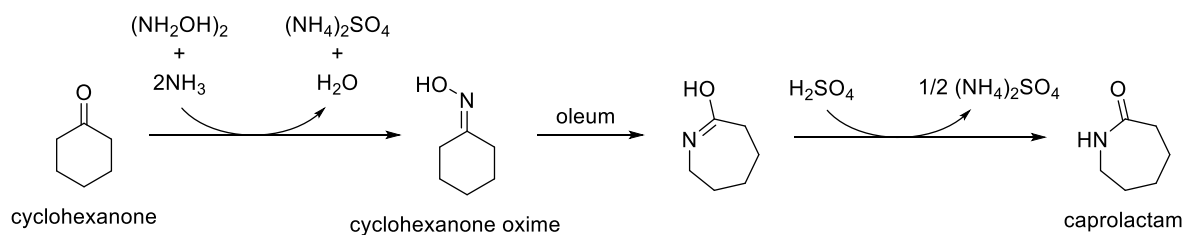

Figure 3. Conventional industrial route to ε-caprolactam using a homogeneous acid catalyst. In the first step, ammoximation of cyclohexanone yields cyclohexanone oxime, which then undergoes the Beckmann rearrangement to form ε-caprolactam.[10]

One of the earliest industrial applications of a heterogeneous catalyst in the Beckmann rearrangement was reported in 1941 when "a practical and continuous method for carrying out the rearrangement of cyclohexanone oxime" using a silica gel catalyst was reported.[11] This concept was developed further, and in 1987 a heterogeneously-catalysed process that proved viable on a scale to rival conventional methodologies was implemented. In 2003, a plant in Niihama (Japan) employing an MFI-type catalyst was made operational, generating 65000 tonnes of ε-caprolactam *p.a.*.[6]

To date, the industrial Beckmann rearrangement remains predominantly a gas-phase process, using a fluidised bed reactor at > 300 $^\circ$C to maintain the solvent (typically ethanol) and both cyclohexanone oxime and caprolactam in the vapour phase. These conditions maximise catalytic activity (> 98 % yield) and lifetime, whilst the continuous nature of the process eliminates catalyst separation steps. The success of the industrial vapour-phase process is also evident in the academic literature (Table 1), where many reports focus on solid-acid catalysts optimised for industrial, vapour-phase conditions.

Table 1. An overview of heterogeneous catalysts with reported activity in the vapour-phase Beckmann rearrangement.

Catalyst	Temperature / $^\circ$C	WHSV / hr^{-1}	Solvent	Conversion / mol%[a]	Selectivity / mol%[b]	TOS / hr[c]	Reference
HP-SAPO-34	325	0.79	ethanol	99	95	6	
SAPO-34	325	0.79	ethanol	63	92	6	[12]
MCM-41	325	0.79	ethanol	15	92	6	
HP-S-1 acid	350	1.5	ethanol	61	95	60	[13]

HP-S-1 calc	350	1.5	ethanol	58	52	60	
S-1	350	1.5	ethanol	25	48	20	
Nb_2O_5/SiO_2	400	17.1	ethanol	99	95	26	[14]
$WO_x/SBA-15$	350	0.6	methanol	75	92	10	[15]
In/SBA-15	350	1.2	benzene	98	97	6	[16]
Bi/SBA-15	350	1.2	benzene	100	100	1	[17]
SBA-15	350	1.2	benzene	64	79	1	
Al/MCM-41	350	2.8	1-hexanol	76	100	60	[18]
Al/MCM-41	420	0.44	ethanol	93	70	7	[19]
P/Al/MCM-41-3	420	0.44	ethanol	97	83	7	
MgAlPO-5	400	3.3	methanol	7	49	1	
SiAlPO-5	400	3.3	methanol	75	66	1	[20]
MgSiAlPO-5	400	3.3	methanol	12	43	1	
S-1 (210 nm)	370	6	ethanol	100	88	4	
S-1 (120 nm)	370	6	ethanol	99	94	4	[21]
S-1 (56 nm)	370	6	ethanol	100	96	4	
MFI nanosheet	350	3	ethanol	69	92	80	[22]
MFI Bulk	350	3	ethanol	18	7	20	
H-Beta	350	0.95	methanol	57	87	8	[23]
H-Beta-NH_3	350	0.95	methanol	96	90	8	

a) Conversion of cyclohexanone oxime, b) selectivity to ε-caprolactam, c) time on stream.

Several reviews deal comprehensively with the early literature pertaining to the commercial Beckmann rearrangement,[24-28] but numerous innovations have been reported in the last decade. In particular, there has been a great deal of interest in developing a more energy-efficient, liquid-phase process that can operate below 150 °C. Whilst the vapour-phase Beckmann rearrangement is high-yielding, it is an energy-intensive process, and the high temperatures tend to promote the formation of unwanted by-products that lower reaction selectivity. Consequently, the development of an efficient, low-temperature process holds much promise, although the technology is currently in its infancy.

Following the success of the gas-phase process,[26] considerable research has been devoted to understanding the properties of heterogeneous acid catalysts that impart a high activity and selectivity in the Beckmann rearrangement.[27] Whilst numerous materials have proven effective in catalysing the rearrangement, the prevalence of zeolites and related porous oxides (silicates, aluminophosphates, etc., referred to as 'zeotypes') is revealing. Such zeotype materials are used widely as solid-acid catalysts, particularly in industrial applications for which their particular physicochemical characteristics are well suited.[27] For example, inorganic porous oxides show excellent mechanochemical stability under a wide range of conditions that, in an industrial setting, translates into long catalytic lifetimes before regeneration is necessary. Most of these favourable attributes arise from their highly-crystalline microporous structures. Such regular porosity (on the scale of a small hydrocarbon molecule) places spatial constraints on molecular diffusion and hence

118   product distribution. When the majority of the active sites are located internally (as opposed to on
119   the surface or at the pore mouths) it is possible to moderate active site accessibility and thus direct a
120   catalytic transformation. This fundamental property of zeotypes is the origin of their inherent
121   reactant and product selectivity. Moreover, by placing the active site within the constrained
122   environment of a microporous network, there is also the possibility of exploiting confinement effects
123   to favour particular transition-states. Several zeolite structures (MFI, BEA, etc.), are known to provide
124   a spatial fit that confers high selectivity in the vapour-phase Beckmann rearrangement.[22,23,29] Due
125   to their potential for industrial implementation, there is significant interest in probing in detail the
126   reaction kinetics and catalyst deactivation processes that operate in these zeolitic systems.[30,31]

127   Whilst microporous zeotypes are renowned for their steric control of reaction mechanism,
128   hierarchical analogues (that possess several levels of porosity) are also receiving considerable
129   interest.[32] These materials have been shown to retain the favourable attributes of the microporous
130   architecture (i.e. well-defined active sites and a good physicochemical stability), whilst
131   simultaneously addressing mass transport limitations.[33] Thus, by incorporating an auxiliary
132   mesoporous network, it is possible to enhance diffusion to and from the internal active sites, thus
133   extending catalytic lifetime by retarding coke-induced deactivation.[13,34]

134   A common synthetic methodology for the production of hierarchical zeotypes involves the
135   addition of a surfactant or oligomeric mesoporogen to the precursor gel.[13,34,35] This bottom-up,
136   soft-templating route is appealing, as it is compatible with conventional one-pot syntheses and the
137   organic mesoporogen is readily removed by the standard calcination protocol. As such, soft-
138   templating has been employed in many instances for the production of hierarchical, zeotype
139   Beckmann rearrangement catalysts. For instance, organosilane surfactants have been shown to
140   integrate with silicoaluminophosphate (SAPO) frameworks so as to yield a homogenous hierarchical
141   phase (Figure 4).[36] Interestingly, in this case the production of mesopores was also accompanied
142   by the formation of localised silanol sites, and the resulting hierarchical SAPO catalysts were found
143   to sustain higher catalytic activity in the vapour-phase rearrangement than their microporous
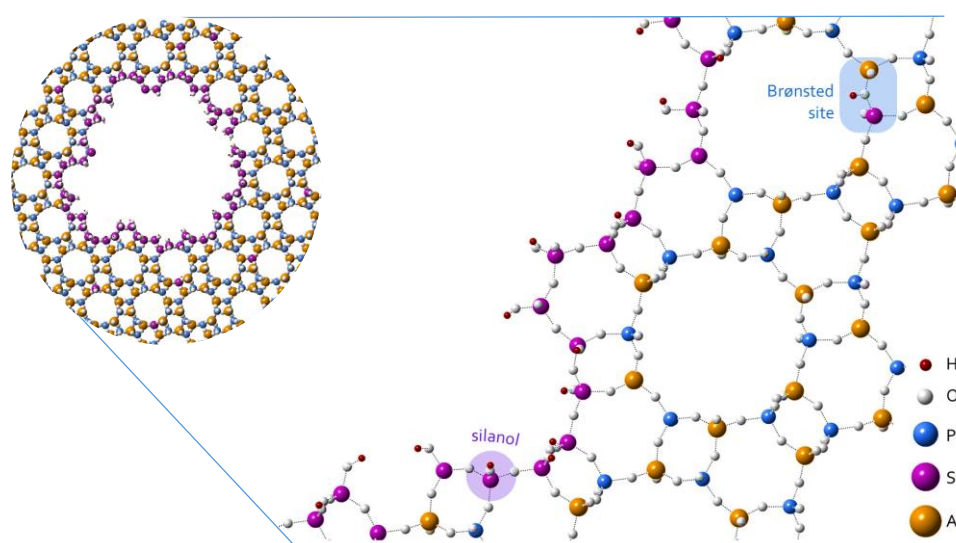144   analogues.

145

Figure 4. Depiction of hierarchical SAPO-5 prepared using an organosilane mesoporogen. The silanol sites are localized to the internal walls of the mesopore, whilst Brønsted acid sites are created in the bulk, microporous framework due to isomorphous substitution of silicon.[36]

Hierarchical SAPO-34 has also been prepared using a novel template system where surfactant encapsulated within MCM-41 acts as both Si-source and mesoporogen.[12] When tested in the vapour-phase Beckmann rearrangement of cyclohexanone oxime, the hierarchical SAPO-34 catalyst maintained high conversion and selectivity over 6 hours on stream, whilst both microporous SAPO-34 and mesoporous MCM-41 showed lower activity and a marked degradation in performance throughout. These results highlight the importance of combining appropriate acid-site characteristics with a favourable framework architecture in order to maximise catalyst efficacy. Another innovative method for creating mesoporous architectures has been presented by Palkovits *et al.*, who used oligomeric siloxane species to cross-link nano-sized particles of TS-1.[37] The inter-particle voids generated by bridging TS-1 particles with amorphous silica were found to improve caprolactam yield under vapour-phase conditions, and also slowed catalyst deactivation. Inorganic templates have also proven to be effective in templating mesoporosity in zeotype Beckmann rearrangement catalysts. For example, $Mg(OH)_2$ nanocrystals added to the synthesis gel yielded hierarchical MFI catalysts with modified textural characteristics. The resultant hierarchical framework showed improved mass transfer properties and enhanced vapour-phase activity compared to the conventional Silicalite-1 catalyst.[38] Beyond the MFI-type systems that are the usual target for vapour-phase Beckmann rearrangement catalysts, other promising systems have emerged. Among these is the microporous titanosilicate ETS-10, the hierarchical analogue of which has been produced, post-synthetically, using a microwave reactor.[29] The microexplosions produced by rapid degradation of hydrogen peroxide created larger pore structures in ETS-10 that boosted catalytic activity in the gas-phase Beckmann rearrangement.

As well as pore structure, the control of particle size is an important consideration in the synthesis of industrial vapour-phase catalysts. This type of manipulation can be achieved in a variety of ways, including modification of the ion content of the synthesis gel. In the synthesis of Silicalite-1, it has been shown that if the concentration of Na^+ and Br^- exceeds 5 mol. % (relative to the structure-directing agent) then larger particles are formed.[39] Despite possessing the same number of strong acid sites, the larger catalyst particles deactivated more rapidly due to greater coke deposition. Silicalite-1 particle size has also been modified *via* synthetic parameters such as ageing time and temperature, water quantity and lysine addition.[21] In this case, Silicalite-1 particles of ~ 50 nm exhibited optimal catalytic activity, selectivity and stability, as coke deposition at the pore mouth and particle surface was retarded. Alternatively, Kim *et al.*, used a novel linear structure-directing agent to create Silicalite-1 nano-sheets of 2 nm thickness. These nano-sheets displayed remarkable activity and lifetime, maintaining a high conversion and selectivity for over 10 times longer than conventional Silicalite-1.[22] Additionally, seed crystals have been used to influence the particle growth of TS-1. Catalyst prepared from nano-sized (100-300 nm) precursor seeds showed greater activity after 6 hours on stream than analogous TS-1 particles templated by micro-sized (4-6 μm) seeds.[40] The benefits of particle control are not confined to vapour-phase catalysts: nano-sized and delaminated zeotypes have also been exploited for the liquid-phase Beckmann rearrangement, where improved

187 active site accessibility is especially advantageous in the transformation of the bulky
188 cyclododecanone oxime substrate.[41]
189   Framework architecture is seminal in zeolite science, and so too is the scope for active site design.
190 Importantly, by combining both attributes appropriately, it is possible to synthesise a catalyst that is
191 targeted towards a desired chemical transformation. For instance, some of the most applicable acid
192 centres are silanol sites: neutral species with a small dipole moment in the Si-O bond that confers
193 weak acidity. These sites are primarily found in zeolites (aluminosilicates) and pure silicates (such as
194 SBA-15 and MCM-41) and are classed as terminal, geminal, vicinal or nest silanols, depending on the
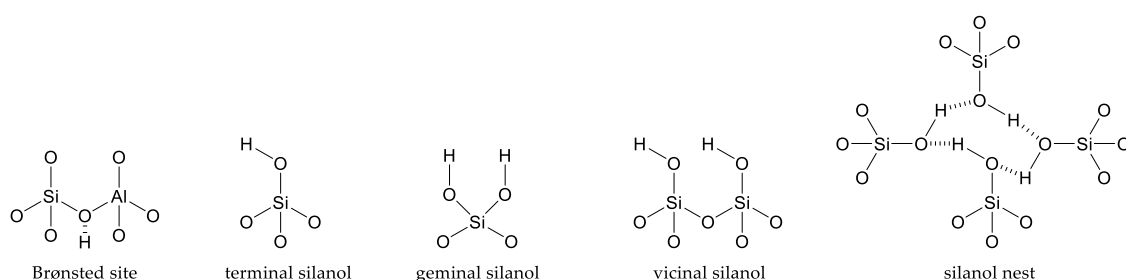195 number of Si-O-Si bonds and their proximity to other silanol species (Figure 5).[42]
196

Brønsted site   terminal silanol   geminal silanol   vicinal silanol   silanol nest

197   **Figure 5.** A depiction of the different types of acid site in zeotype materials.[42]

198   Intrinsically, silanols occur as framework defects, although their precise properties typically
199 reflect the topology and Al/Si ratio of the material. In addition, there are a wide range of post-
200 synthetic treatments that can be used to modify the type and concentration of silanols, and hence
201 increase catalytic potential. For example, silylation of NbO_x/SiO_2 catalyst was found to improve ε-
202 caprolactam selectivity and catalyst lifetime in the gas-phase Beckmann rearrangement. By
203 passivating the more acidic, isolated-silanol sites with hexamethyldisilazane, the catalyst was more
204 resistant to coking, and oxime hydrolysis in the presence of water could be suppressed.[14] Another
205 common post-synthetic procedure involves the removal of framework atoms by treatment with an
206 acid or base. Desilication by this route disrupts the crystalline microporous framework, creating
207 disordered mesopores and defects as new silica surfaces are developed. When ZSM-5 catalysts of
208 varying Si/Al ratio were subject to desilication under basic conditions, the resulting hierarchical
209 zeolites exhibited improved yield of caprolactam in the liquid-phase Beckmann rearrangement due
210 to improved mass transport capabilities. Whilst the synthetic methodology was found to remove a
211 fraction of Brønsted sites, their acid strength was not modified by the procedure.[43] Equally, the
212 selective removal of tetrahedral framework-aluminium (i.e. dealumination) creates silica nests that
213 stabilise silicon atoms adjacent to the Al vacancy, although strong treatments can disrupt framework
214 crystallinity. Ngamcharussrivichai *et al.* showed that a mild acid treatment could be used to enhance
215 the activity of USY zeolite in the liquid-phase Beckmann rearrangement, whilst retaining framework
216 crystallinity. Whilst dealumination was found to increase the concentration of favourable Brønsted
217 acid sites, the creation of Lewis-acidic, extra-framework aluminium species was found to accelerate
218 the formation of cyclohexanone side-product.[44]
219   For commercial Beckmann-rearrangement catalysts, framework modifications focus
220 predominantly on moderating acid or textural properties to improve catalytic activity and minimise

221 coke deposits. In this context, Zhang *et al.* described the treatment of zeolite-β with aqueous ammonia
222 solution to maintain a constant Si/Al ratio (and hence strong-acid site concentration), whilst
223 increasing the amount of weak acid sites four-fold.[23] As a result, the NH$_3$-modified zeolite-β
224 showed a significant increase in catalytic lifetime, and achieved a caprolactam yield of 86 mol. % after
225 8 hours, an increase of 36 mol. % over the standard zeolite-β system. In contrast, under liquid-phase
226 conditions stronger acid sites are crucial if meaningful conversions are to be achieved. Purely-
227 siliceous zeolites with only weak, external silanols are essentially inactive in the Beckmann
228 rearrangement at 130 °C and instead promote oxime hydrolysis.[45] If stronger internal silanols (and
229 the potential for substrate pre-activation by pore confinement) are introduced, moderate activity is
230 observed under the same conditions. Finally, when Al is incorporated to form a zeolite framework,
231 the resulting Brønsted acid sites create a vast improvement in both conversion of oxime and amide
232 selectivity. Even wider scope for the catalytic application of zeotype materials been achieved by the
233 isomorphous substitution of heteroatomic active sites. By doping into a crystalline network at low
234 concentration, a distribution of well-defined, spatially-isolated active sites is created in what is
235 described as a single-site heterogeneous catalyst (SSHC).[46] By this route, a variety of metal dopants
236 have been incorporated into zeotypes, each of which respond to the structural and chemical
237 environment of the framework to create a unique active site. This phenomenon has been exploited in
238 a wide range of zeotype species, perhaps most notably in the aluminophosphates (AlPOs). AlPOs are
239 particularly amenable to isomorphous substitution (Figure 6), since the ionicity of the framework
240 imparts flexibility to bond lengths and angles. Furthermore, AlPOs possess two markedly different
241 T-sites (Al^{3+} and P^{5+}), which offers additional scope for isomorphous substitution.
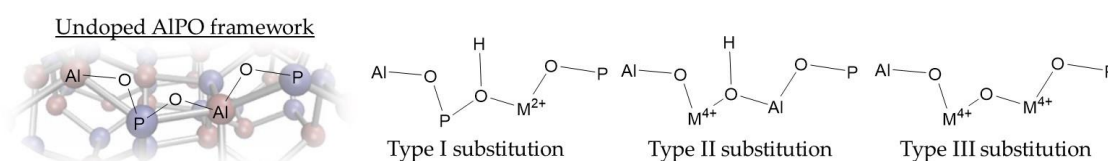
242

243 **Figure 6.** Three mechanisms of isomorphous substitution are observed for AlPO frameworks,
244 depending on the formal charge of the dopant atom. M$^{2+/3+}$ species tend to undergo Type I substitution
245 of Al^{3+}, whereas M$^{4+/5+}$ preferentially replace P^{5+} by Type II. If a pair of M^{4+} species simultaneously
246 substitute adjacent Al^{3+} and P^{5+} to create a M^{4+}-O-M^{4+} bridge, this is designated a Type III substitution.

247 By this route, more than 25 main group and transition elements have been incorporated into
248 AlPO frameworks.[47] In all cases, the formal oxidation state of the dopant heteroatom is the same,
249 or lower than the framework atom it replaces. In the case that the formal charge of the dopant atom
250 is less than the atom it replaces (e.g. Co^{2+} substituting Al^{3+}, or Si^{4+} substituting P^{5+}), the framework
251 develops a net negative charge that must be balanced by a countercation. Typically, the cation is a
252 framework-bound proton, with acidic properties that reflect the local atomic environment, namely
253 the nature and location of the dopant atom, and the topology and composition of the framework. The
254 Brønsted acid sites that arise through isomorphous substitution are typically much stronger than the
255 aforementioned silanols; a characteristic that has been central in the development of catalysts for the
256 Beckmann rearrangement.

257 Through adroit selection of the dopant species, it is possible to create targeted active sites, as is
258 demonstrated in our own work. We found that by doping AlPO-5 with Mg^{2+} stronger acid sites are
259 created – to the detriment of vapour-phase activity. In contrast, the Si^{4+}-doped analogue (SAPO-5)
260 contained significantly weaker acid sites that proved well-suited for catalysing the transformation
261 (Figure 7).[48] Significantly, by combining the strong acid sites from Mg^{2+}-doping, with the weaker
262 acid sites from Si^{4+}-doping, it was possible to create a bimetallic system of intermediate acidity that
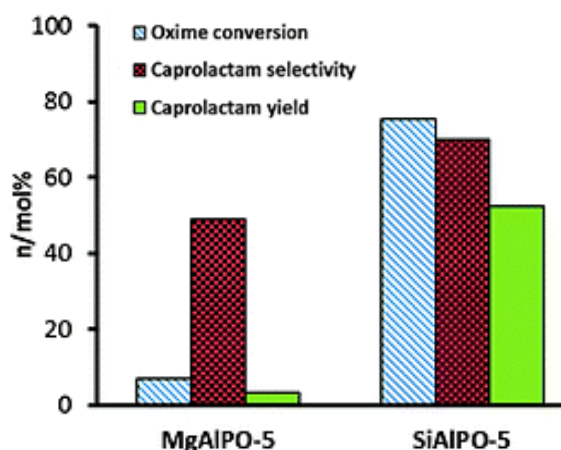263 showed improved caprolactam yield in the vapour-phase.[20,49]
264

265 **Figure 7.** Activity of Mg- and Si-doped AlPO-5 in the vapour-phase Beckmann rearrangement of
266 cyclohexanone oxime (WHSV 3.3 h^{-1}, He carrier gas 20 mL min^{-1}, 0.3 g catalyst, liquid feed 300 g L^{-1}
267 of cyclohexanone oxime in methanol, 673 K).[48]

268 The aluminium-doped, mesoporous silica, Al-MCM-41, has also proven to be of great interest as
269 a Beckmann rearrangement catalyst, since improved mass-transport behaviour has been linked to
270 enhanced caprolactam selectivity and catalytic lifetime. Vaschetto *et al.* have demonstrated that, in
271 the vapour-phase, the weak acidity of nest silanols endows a superior selectivity towards
272 caprolactam.[50] On increasing the aluminium content of Al-MCM-41 (above a critical Si/Al = 60),
273 these silicon nest sites were proliferated, with a concomitant increase in product yield.[51]
274 Furthermore, by pre-treating the catalyst with linear alcohol (1-hexanol) the more acidic terminal
275 silanol sites could be pacified as alkoxy groups, improving lactam selectivity further.[18] Quite
276 contrastingly, in the liquid-phase, the surface silanol groups of mesoporous silicates are too weak to
277 catalyse the Beckmann rearrangement. Thus, under mild reaction conditions, the activity of MCM-
278 41, SBA-1 and SBA-15 could be enhanced by creating stronger acid sites through Al-doping.[52]
279 Moreover, if Al was incorporated by post-synthetic grafting, the bound trigonal-chloride species
280 yielded strong Lewis and Brønsted acid sites that showed better activity in the liquid-phase. Despite
281 showing a high initial activity, the adsorption of caprolactam to the stronger acid sites of Al-grafted
282 MCM-41 accelerated catalyst deactivation.
283 Not all elements are disposed towards isomorphous substitution as the framework often places
284 restrictions on the size or charge of atoms that can be incorporated. Nonetheless, active species may
285 otherwise be accommodated as extra-framework species. In fact, even those atoms eligible for
286 framework substitution can be made to occupy extra-framework sites, provided an appropriate

287 synthesis procedure is adopted. For example, in an effort to dope Zn^{2+} ions into AlPO-5, extra-
288 framework species have been created.[20,48] Whilst, these extra-framework sites did not provide
289 additional catalytic capabilities, their presence was found to modify the acidity of Mg- and Si-doped
290 AlPO-5 systems antagonistically. Thus, bimetallic ZnSiAlPO-5 was found to possess stronger acid
291 sites than SiAlPO-5, whilst MgZnAlPO-5 possessed weaker acid sites than MgAlPO-5. Therefore,
292 extra-framework zinc species proved to be a valuable modifier that could be exploited to improve
293 the yield of caprolactam obtained in MgZnAlPO-5 *versus* MgAlPO-5.

294 It is also possible to use post-synthetic methodologies to introduce non-metallic species into
295 hexagonal mesoporous silicates (HMS). For example, using H_3PO_4 precursors, phosphorus has been
296 successfully impregnated into the Al-MCM-41 framework.[19] After 7 hours on-stream, the activity
297 of the phosphorus-modified catalyst was found to exceed that of the parent Al-MCM-41 due to the
298 combined effect of amplifying the number weak acid sites, whilst simultaneously reducing the
299 quantity of stronger acid sites. Contrastingly, when boric acid was used to prepare an analogous
300 boron-modified Al-MCM-41, catalytic activity in the vapour-phase rearrangement was attenuated by
301 carbonaceous deposits, particularly at the strongest acid sites.[53] Under liquid-phase conditions,
302 increasing the acid strength of Al-MCM-41 and Al-SBA-15 by applying a sulfonic acid ($-SO_3H$)
303 modification has proven to be beneficial to catalyst performance.[54] Nb/SiO_2 systems containing
304 extra-framework NbO_4-tetrahedra have also proven to be highly effective catalysts for the Beckmann
305 rearrangement.[55-58] TEM imaging has revealed the presence of extra-framework niobium sites at
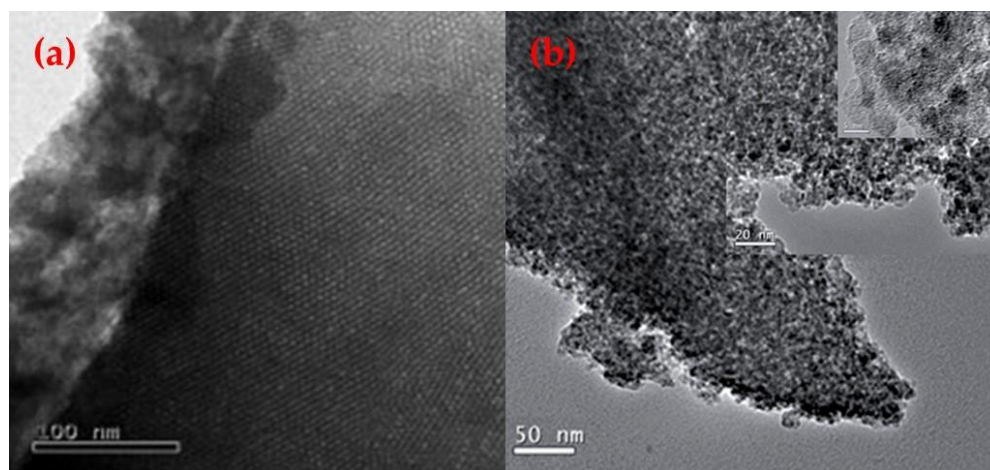306 higher loading, with Nb-clustering favoured over framework substitution (Figure 8).[55]

307

308 **Figure 8.** TEM images contrasting the mesoporous framework-substituted Al-MCM-41 species (a),
309 [43] with the extra-framework Nb sites in Nb/HMS-X (Si/Nb = 2).[55]

310 When a small quantity of niobium (< 0.3 wt. %) is introduced on to a silica matrix, isolated NbO_4
311 species are formed.[55] Whilst the resulting Nb/SiO_2 system lacks the inherent Brønsted acidity
312 typically sought in Beckmann rearrangement catalysts, such activity can be developed by reacting
313 the Lewis-acidic Nb centres with ethanol, *in situ*. Raman and FTIR studies have shown that the
314 interaction of Nb=O groups with co-solvent creates active $NbO_3(OEt)OH$ species that confer Brønsted
315 acidity for the rearrangement.[14,59] In kinetic studies, both the adsorption energy of cyclohexanone
316 oxime (154 kJ mol^{-1}) and the activation energy for the Beckmann rearrangement (68 kJ mol^{-1}) were
317 found to be considerably lower than for the conventional Silicalite-1 catalyst.[56] Nb-doped materials

318　have also proven active under liquid-phase conditions. A Nb-MCM-41 catalyst containing both
319　tetrahedrally-coordinated framework Nb and extra-framework Nb_2O_5 species was used to catalyse
320　both the ammoximation of cyclohexanone and subsequent Beckmann rearrangement in a one-pot
321　reaction at 80 °C.[60] A higher Nb content was found to improve caprolactam yield by increasing
322　catalyst acidity from weak to medium strength, however after optimising reactions conditions, only
323　a 7.3% conversion of cyclohexanone and 66 % selectivity for caprolactam was reported.

324　　Indium, bismuth and tungsten species have also been grafted on to mesoporous silicas to induce
325　catalytic activity. In the case of indium[16] and bismuth,[17] it is proposed that the Lewis acidic metal
326　interacts with the oxygen atoms of proximal silanol species, enhancing the acidity of the latter. In this
327　case, improvements to catalytic activity and lifetime were found to be most prominent when the
328　quantity of metal was very low (~ 3.5 wt. %). However, in the case of WO_x/SBA-15,[15] temperature-
329　programmed desorption revealed that a higher quantity of WO_x yielded more medium-strength acid
330　sites, which translated into improved catalytic performance and sustained activity on regeneration.

331　　It is the sheer scope for structural and chemical functionality in zeotype materials that make
332　them excellent candidates for performing the acid-catalysed Beckmann rearrangement.
333　Fundamentally, these materials offer a robust, porous framework with tuneable acid characteristics,
334　although designing an effective solid-acid catalyst requires an understanding of the nature of the
335　active site, the catalytic pathway and the role of the host. Correspondingly, the literature pertaining
336　to the characterisation of catalysts for the Beckmann rearrangement is extensive. Whilst a host of
337　spectroscopic techniques have been exploited in order to study catalyst structure and mechanism, *in*
338　*situ* and *in operando* techniques in particular have provided opportunities to probe the interactions
339　between active sites and reactive species in a more representative chemical environment. These
340　studies emphasise the importance of comprehensively evaluating the structure-property
341　relationships that elicit catalyst activity, and highlight the profound link between catalyst
342　performance and a controlled catalytic environment.

2. Vibrational Spectroscopy

344　　In the development of heterogeneous catalysts for the Beckmann rearrangement, considerable
345　research has been devoted to optimising framework acidity to maximise caprolactam yield. Effective
346　catalysts bind the oxime substrate with sufficient affinity to promote the desired transformation, yet
347　not so strongly as to retain the lactam product. As a result, acid-site characterisation has become
348　inextricably linked with catalyst design, as is illustrated by infrared (IR) spectroscopy.

349　　IR is a well-established vibrational technique that is widely employed in catalysis for both
350　materials characterisation and *in situ* studies. A range of IR technologies are available, making it an
351　inclusive and informative technique. Commonly, IR spectroscopy is performed in transmission-
352　mode, whereby infrared radiation is propagated through a sample whilst the frequency of resonant
353　absorption of vibrational modes is monitored. However, where transmission IR is incompatible with
354　a (for example, strongly-absorbing) sample, a reflectance protocol may be adopted. Such techniques
355　include Diffuse Reflectance Infrared Fourier Transform Spectroscopy (DRIFTS) and Attenuated Total
356　Reflectance Infrared Spectroscopy (ATR-IR); surface-sensitive methods that are suited to studying
357　chemistry occurring at the interfaces. The wide applicability of the IR technique has led to its
358　integration as part of routine analysis for ascertaining the nature, quantity and strength of the acid

359 sites in a framework, and from this, structure-property relationships have been extrapolated. In
360 addition, by employing more advanced methodologies, such as probe-based techniques or
361 combinatorial studies (e.g. DRIFTS-XAS) it is possible to monitor synchronous changes in the catalyst
362 and surface species under *in situ* or *in operando* conditions.

363 Unsurprisingly, in a review of the literature pertaining to catalysts for the Beckmann
364 rearrangement, IR studies are pervasive. In its simplest form, IR spectroscopy is used to characterise
365 framework acidity based on hydroxyl stretching modes in the 3000-3800 cm^{-1} range. In this region,
366 the precise position of an O-H stretching band is informative of the acid site characteristics, being
367 sensitive to local variations in bond length and angle, and the electrostatic influence of the
368 coordination environment. For the same reason, infrared spectra also exhibit a topological
369 dependence that can be used to distinguish the same type of active site in different framework
370 locations (Table 2). For example, microporous SAPO-34 exhibits two characteristic O-H stretching
371 bands (at 3633 and 3610 cm^{-1}) that have been attributed to two types of Al(OH)Si Brønsted sites.[36]
372 Here, the band at 3633 cm^{-1} arises from a proton attached to the O(4) framework oxygen (which
373 resides in one four-membered and two eight-membered rings), whilst the peak at 3610 cm^{-1}
374 corresponds to a proton bond to the O(2) oxygen (which resides in one four-membered, one six-
375 membered and one eight-membered ring).[47]

376 **Table 2.** Assignment of the FTIR hydroxyl stretching modes (ν(OH)) of SAPO materials and their
377 shift ($\Delta\nu$(OH)) following CO adsorption. The activity of the SAPO catalysts in the vapour-phase
378 Beckmann rearrangement is also reported.

Material	Site	ν(OH) / cm^{-1}	ν(OH$\cdot\cdot$CO) / cm^{-1}	$\Delta\nu$(OH) /cm^{-1}	Catalytic activity in the vapour-phase Beckmann rearrangement at 1 hour		
					Conversion of cyclohexanone oxime / %	Selectivity for caprolactam / %	Reaction conditions
SAPO-37 [61]	Al–OH/P–OH	3680	-	-	> 99	86	300° C, WHSV 0.3 hr^{-1}, He flow 33.3 mL min^{-1}
	Si(OH)Al	3641					
	Si(OH)Al	3575	-	-			
SAPO-34 [36]	Si-OH	3746	-	-	92	70	325° C, WHSV 0.79 hr^{-1}, He flow 33.3 mL min^{-1}
	Al–OH/P–OH	3678	-	-			
	Si(OH)Al	3633	3347	286			
	Si(OH)Al	3610	3281	329			
SAPO-5 [36]	Si-OH	3746	-	-	71	76	325° C, WHSV 0.79 hr^{-1}, He flow 33.3 mL min^{-1}
	Al–OH/P–OH	3678	3368	270			
	Si(OH)Al	3638	3369	268			

379
380 The nature of high-yielding active sites in solid-acid, Beckmann rearrangement catalysts has
381 been the subject of much debate. The consensus is that (unlike the industrial homogeneous system)
382 in the vapour-phase, production of caprolactam is favoured when a heterogeneous catalyst is only

very weakly acidic. Evidence to this effect has largely arisen from the concerted effort to characterise and optimise the industrially-favoured, high-silica MFI zeolite catalyst.

The hydroxyl stretching region of the H-ZSM-5 zeolite, which has been well-characterised by infrared spectroscopy,[62] exhibits two key bands. An absorbance at ~3720 cm^{-1} indicates terminal hydroxyls, identified by ammonia-TPD as weaker acid sites that are supposedly derived from surface termination and framework defects. The other peak at 3600 cm^{-1} is a characteristic framework mode of the MFI zeolite and arises due to the presence of Brønsted acid sites. As is typical of zeolites,[63] the stretching frequency of this mode varies linearly with the Si/Al ratio,[64] and hence framework acidity.[65]

When a range of MFI framework constitutions were studied for activity in the Beckmann rearrangement, it was found that caprolactam yield was maximised using high-silica MFI catalysts (Figure 9). In their study, Sato *et al.* noted that exceptional catalytic activity was obtained at Si/Al > 2000, when the strongest Brønsted acid sites were no longer detectable by ammonia-TPD. Even pure-silica MFI (Silicalite-1) was found to catalyse the Beckmann rearrangement with 100 % conversion and 80 % selectivity for ε-caprolactam. Thus, it was concluded that the Brønsted sites arising from Al incorporation were not the active sites for the vapour-phase Beckmann rearrangement, rather it was the very weakly-acidic, or otherwise neutral silanol sites that were responsible for this activity.[66,67]
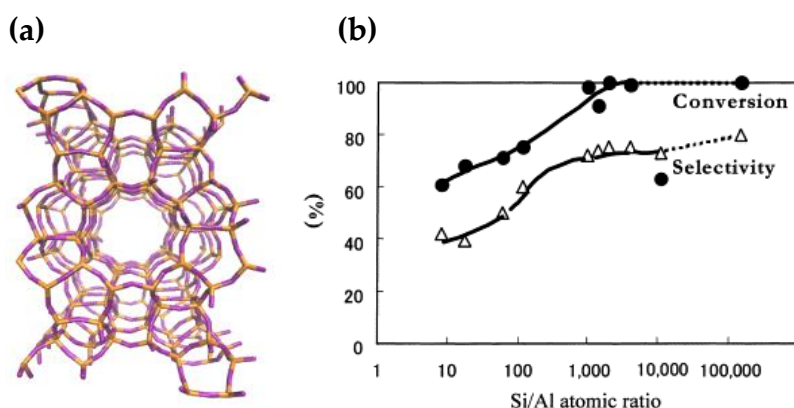
(a)   **(b)**

Figure 9. The MFI structure of Silicalite-1 (*a*), and the influence of Si/Al ratio on the conversion of cyclohexanone oxime (•) and selectivity to caprolactam (▵). Reaction conditions: cyclohexanone oxime (8 wt. %) in benzene solution, WHSV = 3 h^{-1}, 623 K (*b*).[68]

In a combined spectroscopic-catalytic investigation of the active sites in siliceous acid catalysts, Hölderich *et al.* were able to characterise the silanol sites of the MFI catalyst that were responsible for high activity in the Beckmann rearrangement.[69] Using FTIR spectroscopy, three types of silanol site were observed: terminal (3740 cm^{-1}), vicinal (3690 cm^{-1}) and nest (3500 cm^{-1}), with acidity decreasing in that order. Whereas crystalline Silicalite-1 presented only terminal sites, its higher-yielding, ammonia-treated analogue,[70] possessed additional vicinal and nest silanol groups. These weaker silanol sites were considered more effective catalytically, as their appearance was accompanied by a marked increase in lactam yield. The results also vindicated previous reports that by purposefully removing silanol groups in H-ZSM-5 catalysts using trimethylchlorosilane, lactam selectivity could be improved from 85 to 95 mol. %.[71] In this case, infrared analysis of the modified catalyst showed a significant decrease in the intensity of the silanol peaks, particularly for the stronger terminal sites, whilst a C-H stretching mode 2970 cm^{-1} was evolved, confirming the methyl-capping. For the same

415 reason, the industrial high-silica MFI is exposed to methanol at high temperature, since capping the
416 more reactive (and acidic) terminal silanols as an alkoxy group improves selectivity for
417 caprolactam.[26,68]

418   IR in its native form is not a quantitative technique. The half-width at half-maximum of a
419 vibration is modified by inhomogeneity in the local environment of the active site (such as framework
420 defects or hydrogen-bonding interactions), as well as anharmonicity in the vibration.[72] Therefore,
421 to perform a quantifiable assessment of an acid site, a knowledge of the extinction coefficient of the
422 corresponding vibrational mode is required. As this is not always practicable, especially for solid-
423 acid systems, IR can be made into a quantitative technique by coupling with probe-based studies.[72]

424   In probe-based FTIR, a catalyst is exposed to a gaseous, basic molecule that interacts with the
425 acid sites in a manner that ranges from hydrogen bonding interactions through to protonation.
426 Suitable probe molecules form a well-known adduct, with characteristic bands in largely
427 unpopulated regions of the IR spectrum.[73] Typically the extinction coefficient of a characteristic
428 probe vibration is known, allowing peak area to be correlated with the concentration of the adsorbed
429 species. Through acid-base interactions, it is possible to assess the strength of the acid site by the
430 degree of red-shift of the framework O-H mode (Δv_{OH}), since stronger acid sites translated to a greater
431 degree by interaction with a probe molecule. It is also possible to quantify active site concentration
432 through the decay of framework bands and/or the growth of characteristic modes of the sorbed probe.
433 Moreover, by monitoring the IR spectrum of the sorbate-adsorbent system over a range of
434 temperatures, the sorptive properties of the probe molecule can be used to determine acid-site
435 strength.[74] In this sense, probe-based IR mimics temperature-programmed desorption (TPD)
436 studies, except that the desorption of the basic molecule is monitored through the loss of its
437 characteristic vibrational modes, rather than by measured desorption.

438   Depending on the nature of the probe molecule, targeted study of acid characteristics is
439 possible.[12] Carbon monoxide is the most widely used probe molecule for zeotype species, as it can
440 readily diffuse through the smallest pores, accessing a wide range of acid sites. Where the frequency
441 of the C≡O stretch is sensitive to the nature and strength of the acid site, it is possible to distinguish
442 different acid sites based on $v(CO)$ (Table 2). However, CO is a weakly-basic molecule and as such,
443 adsorption will only occur at acid sites of sufficient strength to maintain an interaction. In contrast,
444 NH_3, a much stronger base, will also interact with weaker acid sites. By employing larger probe
445 molecules (such as pyridine, lutidine or collidine), it is possible to approximate the location of the
446 acid sites within a framework. Due to their larger kinetic diameter, bulky probe molecules will only
447 interact with acid sites that are made accessible by the pore structure and the proximity of other
448 available active sites. Thus, it is common practice to use a range of probe molecules to obtain a more
449 comprehensive understanding of the location and strength of the acid sites. By extension, if the probe
450 molecule is also the reactive substrate, it is possible to monitor, *in situ*, the active sites that participate
451 in catalysis and hence determine catalyst mechanism. Such was the basis of an *in situ* FTIR study by
452 Flego and Dalloro, who investigated the activity of weak silanol nest sites in the Beckmann
453 rearrangement.[74] By tracking the adsorption and transformation of cyclohexanone oxime on
454 Silicalite-1 using FTIR, the authors found direct evidence for the involvement of silanol active sites in
455 the transformation to lactam, and used this to establish a reaction mechanism. Fundamentally, the
456 interaction of multiple hydroxyl groups within a silanol nest orients the oxime substrate in a reactive
457 conformation that preserves cyclic geometry and stabilises the intermediate species. In contrast, the

458 more acidic, isolated silanols were found to strongly adsorb both the oxime and lactam, to the
459 detriment of reaction selectivity.

460 Given the compelling evidence in favour of weak acid sites for the vapour-phase Beckmann
461 rearrangement, heteroatom-doped AlPOs have since been investigated. These materials allow single-
462 sites to be engineered with desirable characteristics through the choice of framework dopant and
463 pore architecture.[42] Whilst there is immense scope for modulating the acid characteristics of
464 heteroatom-substituted AlPOs to target the Beckmann rearrangement, the importance of dopant
465 identity has been illustrated in our earlier work comparing the performance of Mg^{2+} and Si^{4+}-doped
466 AlPO-5 (AFI).[48] Using carbon monoxide and 2,6-dimethylpyridine in probe-based FTIR studies, it
467 was possible to correlate the poor yield of caprolactam obtained using MgAlPO-5 with the presence
468 of strong acid sites. It was proposed that these stronger sites retain the lactam product more strongly,
469 impairing selectivity. In contrast, SiAlPO-5, which was found to possess a greater proportion of
470 weaker acid sites, gave superior performance in vapour-phase process. More recently, Gianotti *et al.*
471 studied the effect of dual-substitution of Mg and Si.[49] The resultant bimetallic MgSiAlPO-5
472 material, which had an acidity intermediate of the monometallic systems (Figure 10), exhibited
473 synergistic enhancements in catalytic activity, with improved yield of caprolactam. These results
474 highlighted further scope for modulating active site strength in AlPOs for optimal activity in targeted
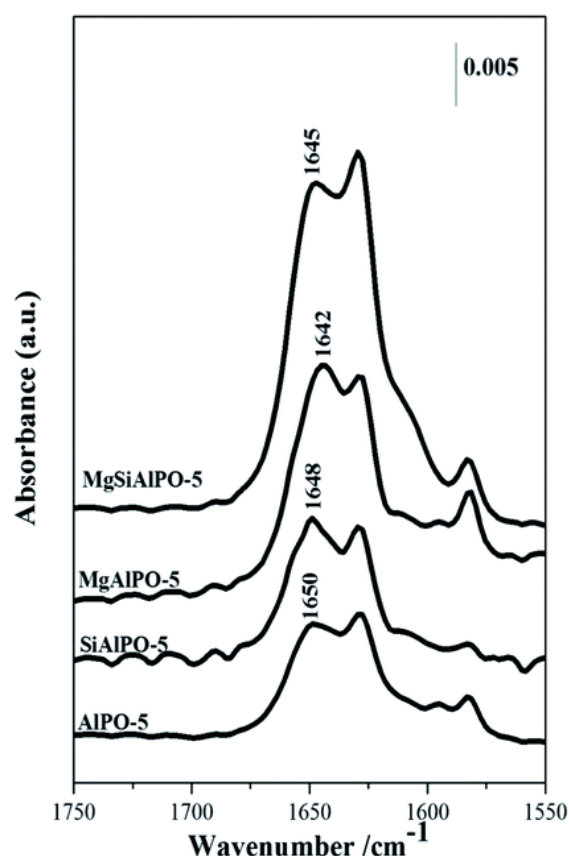475 transformations.

476
477 **Figure 10.** The FTIR spectra of 2,6-dimethylpyridine dosed on AlPO-5 and heteroatom-substituted analogues,
478 shown at 298 K and after degassing. The relative peak position of the ν_{8a} mode (the labelled peak in the 1655–1640 cm^{-1}
479 range) reveals the intermediate strength of MgSiAlPO-5, since a lower wavenumber correlates with stronger Brønsted
480 acid sites.[49]

481   In general, SAPOs have proven well-suited for catalysing the vapour-phase Beckmann
482 rearrangement on account of their weak, tuneable acidity.[12,36,75] Recently, hierarchically-porous
483 (HP) SAPOs have been engineered to combine the desirable physicochemical characteristics of the
484 microporous material with an auxiliary mesoporous network in order to enhance diffusion and
485 catalyst longevity. In our previous work, Newland *et al.* describe soft-templating to introduce
486 mesoporosity into microporous SAPO frameworks.[36,76] The FTIR technique (amongst others) was
487 used to characterise Brønsted sites (3628− 3600 cm^{-1}) arising from the isomorphous substitution of Si
488 into HP SAPO-34 and HP SAPO-5 frameworks. In addition, the vibrational spectra of these catalysts
489 revealed a band at 3746 cm^{-1}, which was absent in their microporous analogues. This mode was
490 attributed to pendant silanol sites within the mesopores, originating from the siliceous surfactant
491 template. It was proposed that the interplay between the weaker silanol sites and the isolated
492 Brønsted centres was responsible for the enhanced catalytic performance of the hierarchical catalysts
493 in the Beckmann rearrangement.
494   Hierarchical SAPO-34 has also been synthesized using surfactant encapsulated within MCM-41
495 as a combined mesoporogen and silicon source.[12] To investigate the nature, strength, and
496 accessibility of the Brønsted acid sites, the hierarchical material was subject to probe-based FTIR. Due
497 to the weak basicity of CO and its ability to permeate the small pores of the framework, the molecule
498 can differentiate acid sites of different strength. In the FTIR spectra of CO adsorbed at 80 K, the
499 hydroxyl stretching of the Brønsted acid sites (3630 and 3610 cm^{-1}) in HP SAPO-34 and SAPO-34 was
500 red-shifted by hydrogen bonding to CO, forming an intense absorption centred at ~ 3350 cm^{-1}. The
501 extent of this red-shift was found to be comparable in both microporous and hierarchical SAPO-34,
502 indicating that their Brønsted acid sites were of similar strength. Similarly, the corresponding C≡O
503 stretching mode was blue-shifted by 32 cm^{-1} through interaction with Brønsted acid sites in both CHA
504 materials. Additionally, for HP SAPO-34 it was possible to differentiate the acid sites within the
505 micropores from those in the mesopores by varying the kinetic diameter of the basic probe. Whilst
506 the sorption of ammonia, like CO, is relatively unhindered, its stronger basicity makes it less
507 discriminative in its interaction with acid sites. Hence, NH$_3$ was used to quantify the total framework
508 acidity. In contrast, bulky substituted-pyridines (with kinetic diameters in excess of the micropore
509 dimensions) can only interact with the acid sites that are accessible within the mesopores or at the
510 micropore mouths. Illustratively, the O-H stretch of the Brønsted acid sites in HP SAPO-34 were
511 found to only partially diminish on exposure to 2,4,6-trimethylpyridine (collidine) vapour,
512 suggesting that only a fraction of these sites were accessible to the molecules. In fact, using probe-
513 based FTIR it was possible to quantify that < 4 % total Brønsted acid sites in HP SAPO-34 were
514 available to the substituted pyridines. Nonetheless, the improved accessibility of the acid sites in HP
515 SAPO-34 resulted in significant enhancement in the yield of ε-caprolactam *versus* SAPO-34, MCM-
516 41, or a mechanical mixture of these phases. Thus, it was emphasised that these bimodal catalysts
517 integrate improved mass transfer with the favourable acid-site characteristics of the microporous
518 framework.
519   SAPO-37, a silicoaluminophosphate with the FAU-type structure has been shown particularly
520 effective in catalysing the liquid-phase Beckmann rearrangement. In SAPO materials, Si can be
521 incorporated into the framework by Type II or Type III isomorphous substitution mechanisms,
522 leading to the formation of isolated Brønsted sites (Type II), or silicon islands (Type II and Type
523 III).[77] Due to a preference for incorporating Si *via* the Type II mechanism,[78] SAPO-37 contains a

largely homogeneous distribution of isolated Brønsted acid sites. This can be advantageous in developing targeted, solid-acid catalysts, since such isolated Brønsted sites are weaker than those produced by silicon islanding. Thus, by controlling the fraction of acid sites generated by Type II substitution, it is possible to tune the acid characteristics of SAPO-37. On this basis, we developed a SAPO-37 catalyst that achieved near-quantitative yield of ε-caprolactam in the liquid-phase Beckmann rearrangement.[79,80] However, it is noteworthy that other systems containing weakly-acidic sites (e.g. MCM-41) show poor activity in the liquid-phase reaction, indicating that (unlike the vapour phase) a certain strength of acid site is required. Using a range of characterisation tools (TPD, ssNMR, INS and FTIR), we studied the effect of Si-loading on the acid characteristics SAPO-37. Due to a preference for site-isolation, at low Si-loading SAPO-37 contained predominantly weak, isolated Brønsted sites. However, on increasing dopant levels, silicon islanding became increasingly prevalent, leading to the formation of stronger acid sites, as revealed by NH_3-TPD. Significantly, selectivity towards the desired lactam product was found to correlate with weaker acidity, and hence lower Si-loadings.[80]

In order to probe the activity of SAPO-37 in the liquid-phase Beckmann rearrangement, the interaction of cyclohexanone oxime with the framework was examined.[79] In this case, the less conventional vibrational technique of inelastic neutron spectroscopy (INS) was employed. Whilst vibrational spectroscopy is a natural choice for the characterisation of surface-bound adsorbate, the sensitivity of optical techniques is often limited by the opacity of the zeolite and an inability to access informative, low-energy modes in the fingerprint region. However, in INS, the SAPO framework is effectively transparent because hydrogen atoms are significantly more effective at scattering neutrons.[81] Thus, INS spectra are dominated by the hydrogenous modes of key catalytic moieties (such as framework hydroxyls and silanols) and reactant species. Remarkably, the INS studies revealed that in a solvent-free environment, caprolactam was formed significantly below the reaction temperature, rationalising the efficacy of the isolated acid sites in SAPO-37 for the liquid-phase Beckmann process (Figure 11). A different neutron technique, quasi-elastic neutron scattering (QENS), was used to study the diffusion of cyclohexanone oxime in SAPO-37.[79] At 373 K, cyclohexanone oxime, in a physical mixture with SAPO-37 catalyst, was found to undergo jump diffusion, with a jump distance of 4.5 Å, corresponding to the separation between the faujasitic supercages. Such behaviour contrasts with Zeolite-Y (FAU), which exhibits smooth, Fickian diffusion of the oxime under the same conditions. We attributed the jump diffusion behaviour to interaction between the oxime and the internal acid sites that facilitate the Beckmann rearrangement. This was corroborated by INS, which revealed concomitant loss of vibrational modes of both the framework hydroxyls and oxime O-H groups when the two species were intermixed. These spectroscopic studies reveal differing interactions between cyclohexanone oxime and the weak acid sites of the SAPO-37 framework, *versus* the stronger sites in its zeolitic analogue. It is the favourable, low-temperature interactions of the Brønsted sites in SAPO-37 that were deemed responsible for the high selectivity towards caprolactam in the Beckmann rearrangement.
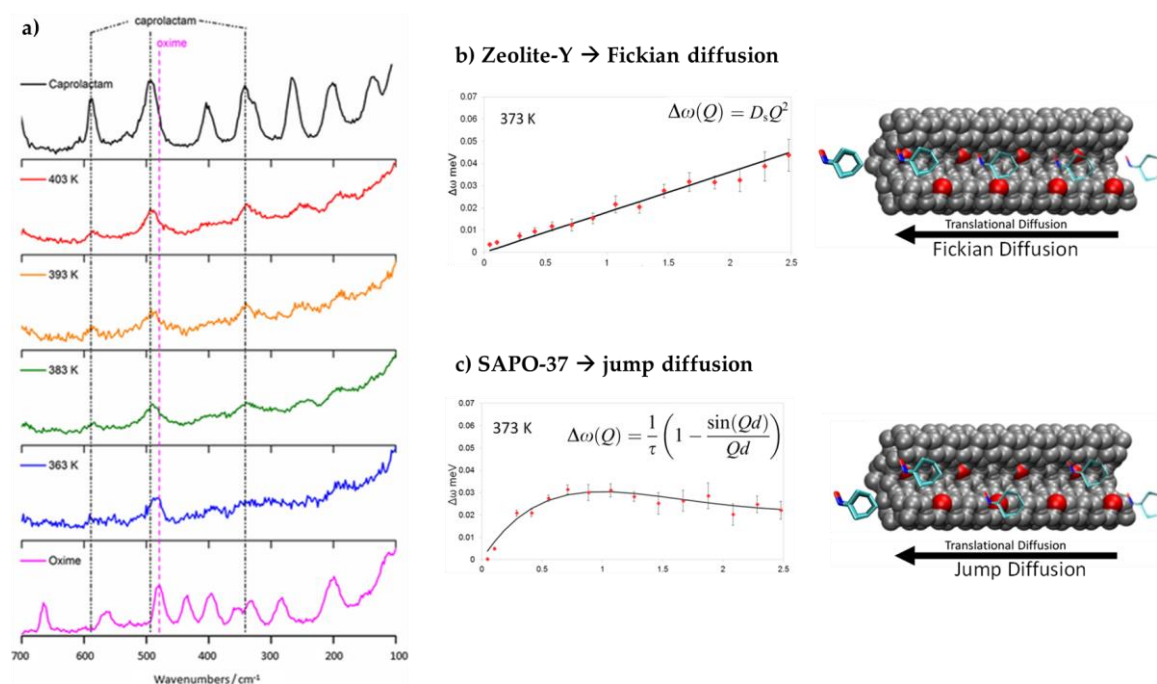
563 **Figure 11.** In a physical mixture of SAPO-37 and cyclohexanone oxime, INS studies revealed that ε-
564 caprolactam was formed significantly below the reaction temperature of 130 °C (**a**).[80] QENS studies
565 revealed that cyclohexanone oxime, in a physical mixture with Zeolite-Y (FAU), exhibits smooth,
566 Fickian diffusion (**b**), whereas in SAPO-37, the oxime is found to undergo jump diffusion due to
567 favourable interaction with the internal acid sites (**c**).[79]

568 **3. Solid-state Nuclear Magnetic Resonance (ssNMR) Spectroscopy**

569 With the development of new technologies such as superconducting magnets and specialised
570 pulse sequences, solid-state (ss)NMR has become an increasingly informative and applicable
571 technique in catalyst characterisation.[82-84] Moreover, increased compatibility with a range
572 experimental conditions has provided greater scope for *in situ* studies of catalyst mechanism, as has
573 been actively demonstrated for the Beckmann rearrangement.

574 Due to the ascendancy of zeotype materials in heterogeneous catalysis, some nuclei are observed
575 more routinely by ssNMR than others. For the purpose of structural characterisation, ^{29}Si NMR is
576 common. The number and type of silanol species within a catalyst can be determined using 1D ^{29}Si
577 magic angle spinning (MAS) NMR, however 2D and cross-polarisation (CP) MAS NMR are also used
578 to resolve discrete environments by exploiting the sensitivity of Si nuclei to neighbouring spin-active
579 nuclei.[80] Common ^{29}Si signals are summarised in Table 3. For purely siliceous frameworks, it is
580 typical to quantify the Q^3 species as these identify with the active sites for the vapour-phase
581 Beckmann rearrangement.

582 **Table 3.** Typical ^{29}Si NMR assignments for zeotype Beckmann rearrangement catalysts.

Material Type	Species			Signal
Silicates [85]	$Si(OSi)_4$	Q^4	Tetrahedral framework silica.	110
	$(HO)Si(OSi)_3$	Q^3	Terminal, nests or bridged silanol.	103
	$(HO)_2Si(OSi)_2$	Q^2	Geminal silanol.	90

Silicon-substituted aluminophosphates [80]	Si(OSi)$_3$(OAl)	T^4	Framework silica with an adjacent Al atom.	108
	Si(OSi)$_2$(OAl)$_2$	T^4	Framework silica with two adjacent Al atoms.	104
	Si(OSi)(OAl)$_3$	T^4	Framework silica with three adjacent Al atoms, typically at the periphery of a silicon island.	101
	Si(OAl)$_4$	T^4	Isolated silicon atom, leading to a Brønsted acid site.	92
Boron-substituted zeolites [86]	Si(OSi)$_3$(OB)	Q^4	Tetrahedral silicon with adjacent boron atom.	110

583

584   Depending on framework constitution, ^{27}Al, ^{31}P and ^{11}B nuclei may also be probed using ssNMR.
585   ^{27}Al NMR is less sensitive than ^{29}Si NMR and as such offers relatively limited information, although
586   it is possible to quantify *intra-* and *extra-*framework aluminium species based on the intensity of AlO$_4$
587   (59 ±2 ppm) and AlO$_6$ (0 ±2 ppm) resonances, respectively.[87] In some cases the penta-coordinate
588   aluminium of surface species may be resolved, however this is challenging without the use of 2D
589   MAS NMR. Similarly, ^{31}P NMR can be used to establish a tetrahedral oxide environment (as in
590   AlPOs), which presents itself as a peak at around -30 ppm.[80,88] NMR analysis of ^{11}B nuclei is more
591   definitive of the structural chemistry of boron-doped systems, differentiating the nucleus as it
592   alternates between tetrahedral coordination (B(OSi)$_4$, -4 ppm) in a hydrated system, and trigonal (5-
593   10 ppm) when dehydrated.[89] Furthermore, boron chemical shift is sensitive to the local atomic
594   environment: a study of B-Ge-ZSM-5 was able to resolve the local environment of boron through a
595   B(OSi)$_4$ signal at -4.1 ppm, B(OSi)$_3$(OGe) at -2.9 ppm, and B(OSi)$_2$(OGe)$_2$ at -1.7 ppm.[90]

596   Solid-state NMR has also been used to study the porosity of framework materials *via* ^{129}Xe
597   NMR.[91-93] In zeotypes, the chemical shift of a ^{129}Xe probe molecule is sensitive to both surface
598   interactions and also the uniformity and connectivity of the pores. By controlling the temperature
599   and pressure of ^{129}Xe adsorption, the textural characteristics of the framework can be established.
600   Moreover, using hyperpolarised 2D exchange NMR spectroscopy (EXSY) on hierarchically-porous
601   systems it is possible to measure the rate at which Xe interchanges between the micropores and
602   mesopores, and hence assess diffusion and pore connectivity (Figure 12).[92] This technique has been
603   used to investigate how post-synthetic treatment of Silicalite-1 affects catalytic activity in the vapour-
604   phase Beckmann rearrangement.[93] In this case, ion exchange and calcination protocols were found
605   to modify the hydroxyl population of Silicalite-1. Specifically, low-pH treatment and higher
606   calcination temperature was found to favour geminal silanol sites, leading to reduced catalyst activity
607   and lifetime. ^{129}Xe NMR chemical shift showed that Xe was interacting less effectively with the pore
608   wall where the higher concentration of Si(OH)$_2$ defects created more space in the pores. Thus, the
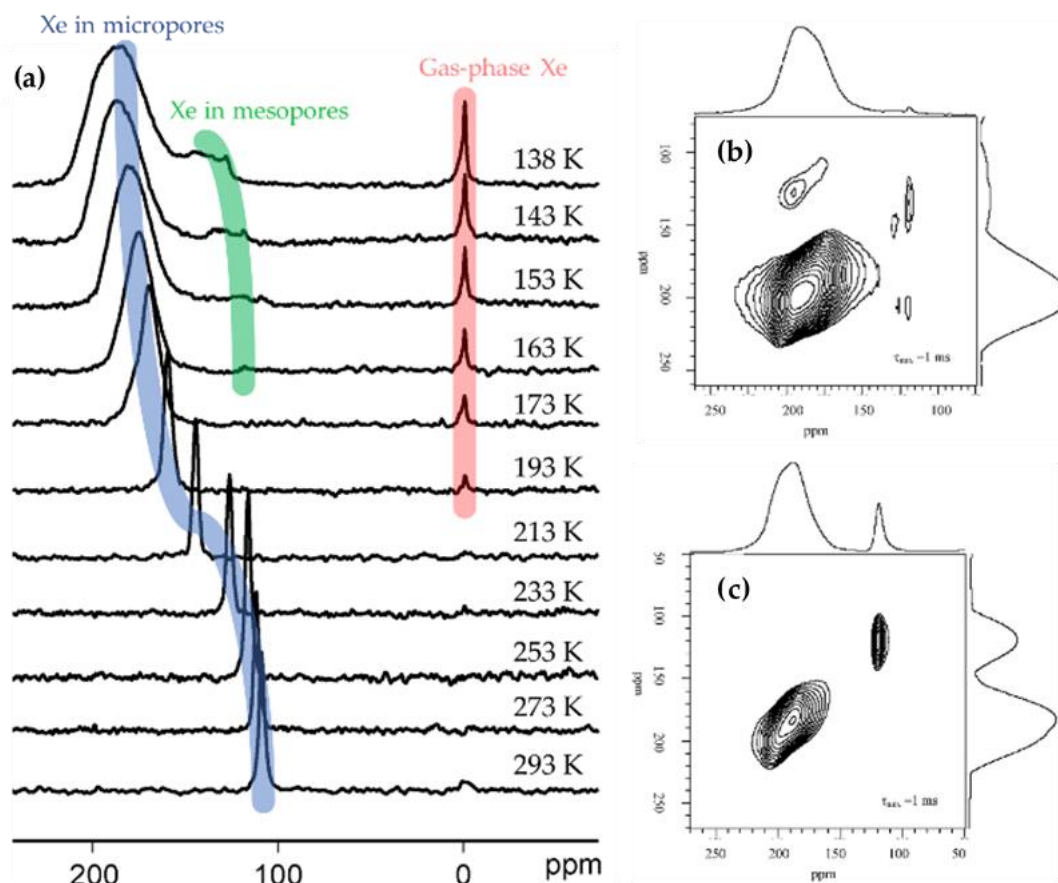609   authors attributed the enhanced catalyst degeneration to enhanced coke formation in the larger
610   pores.[93]

Figure 12. [129]Xe NMR of Meso-ZSM-5 (50) between 293 and 138 K, showing the presence of Xe with different spatial constraints (**a**). Laser-hyperpolarised [129]Xe 2D-EXSY NMR with a mixing time of 1 ms of Meso-ZSM-5 (50) at 143 K (**b**). Off-diagonal signals are due to Xe transferring between micropores ($\delta \sim 200$ ppm) and mesopores ($\delta \sim 120$ ppm). Laser hyperpolarised [129]Xe 2D-EXSY NMR of a physical mixture of microporous ZSM-5 and mesoporous silica at 143 K, with a mixing time of 1 ms (**c**). A lack of off-diagonal peaks indicates slower diffusion of Xe between the micropores ($\delta \sim 200$ ppm) and mesopores ($\delta \sim 120$ ppm).[92]

To directly probe the acid sites in zeotype materials ^{1}H MAS NMR may be employed.[89,94,95] Using this technique it has been possible to distinguish Brønsted acid protons (4.0 ppm) and silanol species (1.8 ppm) in mordenite zeolites.[96] However, assigning bands can be challenging, especially where multiple proton environments exist in a single system. Moreover, the chemical shift of a particular acid site will vary between frameworks as the local environment of the proton changes. In analogy with probe-based FTIR, it is also possible to characterise acid sites by their interaction with a probe molecule, by tracking the ^{1}H NMR signal as pressure or temperature is varied. For example, boron-substituted ZSM-5 (H-[B]ZSM-5) was subject to the adsorption of basic probe molecules and studied by ^{1}H and ^{11}B MAS NMR spectroscopy.[89] In the proton spectrum of the dehydrated H-[B]ZSM-5, three signals due to silanol groups (1.9, 2.5 and 3.2 ppm) were identified. However, on adsorption of ammonia and pyridine the signal at 2.5 ppm was diminished, allowing the assignment of acidic bridging-hydroxyl groups adjacent to a framework boron atom (SiO(H)B). Where ssNMR revealed that the proton affinity of H-[B]ZSM-5 was greater than its aluminosilicate analogue, it was possible to establish the weaker acidity of SiO(H)B groups *versus* the SiO(H)Al Brønsted sites of the zeolite.

633   The technique of ^{1}H ssNMR has also been extended to *in situ* studies of substrate-framework
634   interactions between cyclohexanone oxime and zeolites. In one such study, the proton environment
635   of Silicalite-1 (MFI, Si/Al = 1700) was contrasted with that of ZSM-5 (MFI, Si/Al = 14).[94] When
636   Silicalite-1 was loaded with cyclohexanone oxime, a resonance due to hydrogen-bonded oxime was
637   identified at 9.3 ppm. On heating, the intensity of this peak was reduced, with concurrent growth of
638   a signal at 12.2 ppm due to hydrogen-bonded caprolactam. In contrast, the more acidic ZSM-5
639   framework (with acidic bridging hydroxyls groups producing a signal at 4.2 ppm), showed both
640   hydrogen-bonded (9.3 ppm) and protonated oxime (11.2 and 13.0 ppm). Subsequent heating of the
641   ZSM-5 system led to a strong decrease in the signals at 11.2 and 13.0 ppm, whilst a peak at 14.2 ppm
642   was evolved due to the formation of protonated caprolactam. Furthermore, ε-aminocaproic acid by-
643   product (identified by the signal of the NH_2 group at ~ 6.5 ppm) was detected in the presence of ZSM-
644   5, due to ring-opening of ε-caprolactam by the stronger acid sites. MAS NMR studies of isotopically
645   labelled oxime substrate have proven to be invaluable in establishing the mechanism of the vapour-
646   phase Beckmann rearrangement (Figure 13).[97-99] Using ^{1}H/^{13}C and ^{1}H/^{15}N cross-polarization MAS
647   NMR, Fernández *et al.* probed the mechanism of the Beckmann rearrangement of isotopically-
648   labelled acetophenone oxime in (siliceous) beta-D and (Al-containing) H-beta-D zeolites.[95] The
649   studies revealed two reaction pathways for the rearrangement, depending on the strength of the acid
650   site. Whilst both silanol and Brønsted sites were catalytically active, the acidity of the silanol groups
651   was insufficient to protonate acetophenone below the transformation temperature (473 K), instead
652   forming hydrogen-bonded complexes. In contrast, the Brønsted sites present in aluminium-doped,
653   H-beta-D zeolite were able to effect *N*-protonation at room temperature.

654   Further insight has been gained by comparing the signals of weakly acidic and neutral catalysts
655   (SBA-15 and Silicalite-1, respectively) with those containing Brønsted acid sites (ZSM-5) to correlate
656   acid-site strength with mechanism pathway. Where weakly acidic species are unable to protonate the
657   cyclohexanone oxime (**A**) to form the *N*-protonated oxime (**B**), reaction does not proceed *via* the 1,2-
658   H shift to the *O*-protonated oxime (**C**). Instead, cyclohexanone oxime forms a hydrogen-bonded
659   adduct with several silanol groups (**D**) that is transformed to the nitrilium ion (**F**). Equally, weak and
660   neutral sites are unable to protonate the caprolactam product (**G**), instead the lactam is physically
661   adsorbed to SiOH sites. In contrast, stronger acid sites tend to produce *O*-protonated (**H**) and *N*-
662   protonated (**I**) lactam product. In the presence of water, this can drive ring-opening reactions to form
663   by-products, such as ε-aminocaproic acid (**J** & **K**). When these experiments were performed in the
664   presence of ^{13}C-labelled methanol, the alcohol solvent was found to react with the strong acid sites to
665   form ethers, alkenes and, more importantly, water, through dehydration reactions. The water was
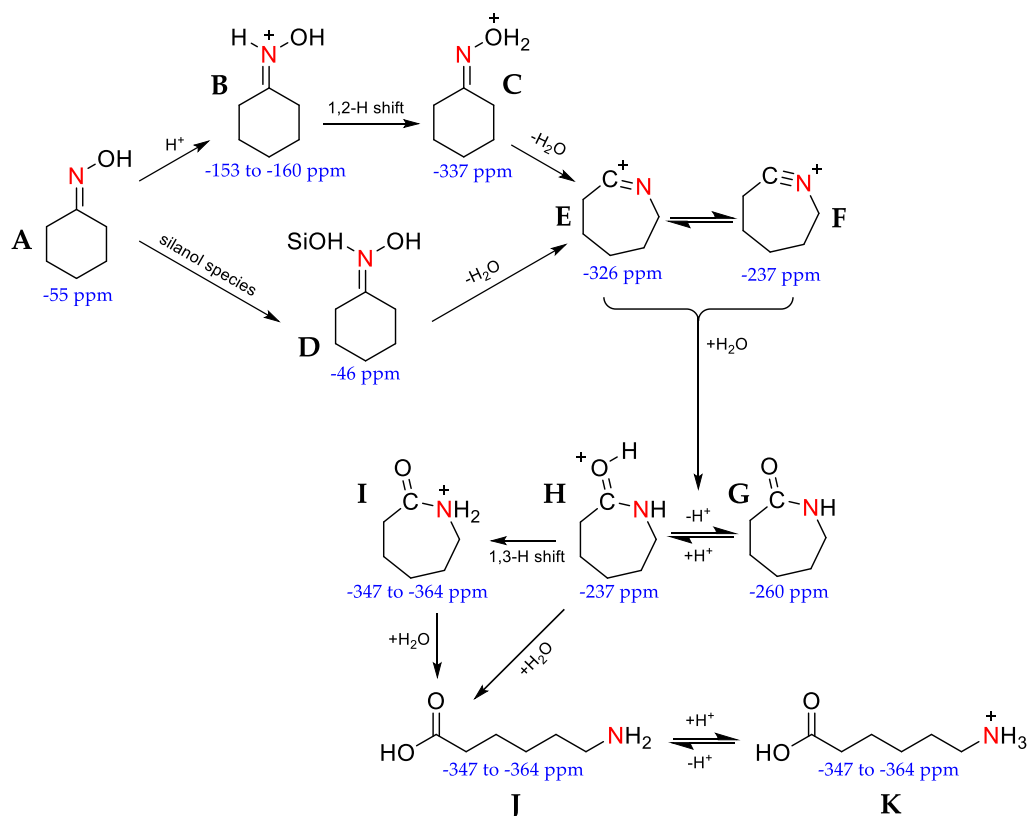666   then available to react with the protonated caprolactam, to the detriment of reaction selectivity.[98,99]
667

Figure 13. The mechanism of the Beckmann rearrangement, determined experimentally using ^{15}N MAS NMR on Silicalite-1 and H-ZSM-5 and ^{15}N-labelled cyclohexanone oxime. The numbers in blue indicate the ^{15}N chemical shifts assigned using DFT modelling.[98,99]

Presently, there remains ample opportunity to perform analogous ssNMR studies on the liquid-phase Beckmann rearrangement, where there is considerable evidence to suggest that the mechanistic pathway deviates from that of the vapour phase. As ssNMR technology continues to improve, a wider range of experimental conditions are becoming accessible, and the use of isotopically-labelled species is allowing greater insights into molecular transformations. For example, ^{17}O NMR, in conjunction with ^{1}H NMR (*via* HETCOR, MQMAS, REDOR and CP techniques), has emerged as a powerful technique for probing oxygen sites. Whilst this technique has not yet been applied to study the Beckmann rearrangement, there is great potential in using ^{17}O NMR to assess parameters such as bond length, acid site location, proton exchange rate, etc..[96] Conceivably, NMR experiments could also be used to improve our understanding of the catalyst deactivation pathways that affect the Beckmann rearrangement, as has already been demonstrated for the methanol-to-olefin process.

4. Computational Insights

Undeniably, innovations in spectroscopic analysis have driven numerous advances in the field of catalysis, both in active site design and mechanistic studies. In tandem with this, an exponential growth in computing power and *ab initio* methods has made it possible to decipher complex catalytic phenomena occurring at an atomic-level. Significantly, by integrating theoretical and empirical studies it has become possible to both predict and rationalise macroscale events at a fundamental level.

690   In the literature, computational studies relating to the Beckmann rearrangement
691 overwhelmingly employ either quantum mechanical (QM) or density functional theory (DFT)
692 methods, with relatively few examples of molecular dynamics (MD) or simulations. However, within
693 the sphere of theoretical science, there are two foci: mechanistic studies (calculating the energetics of
694 intermediates and transition states, in both gaseous media and within confined pores) and the
695 interpretation of characterisation data (calculating chemical properties of reaction intermediates and
696 assigning spectral signals). Other areas of study, such as kinetic modelling or catalyst deactivation,
697 are reported far more infrequently for the Beckmann rearrangement.

698   Initially, QM calculations for the acid-catalysed Beckmann rearrangement used gas-phase
699 species (i.e. single, isolated molecules with no confinement effects or host framework) to corroborate
700 the four key steps of the experimentally-derived mechanism: *N*-protonation of the oxime, 1,2
701 hydride-shift, rearrangement and tautomerisation. Other studies performed under these conditions
702 have offered additional insights into the Beckmann process, for example how aprotic solvents
703 promote by-product formation through hydrolysis of oxime starting material,[100] or how the
704 presence of water lowers the activation energy of the rate-determining step (RDS).[101] Whilst
705 insightful, these early gas-phase studies tended to over-estimate activation energies to approximately
706 double that determined experimentally ($\sim$ 200 kJ mol^{-1} compared to $\sim$ 100 kJ mol^{-1}) for zeotype
707 systems.[101] Such values are typically obtained by specifying a reaction-coordinate (such as a bond
708 length) and constructing a reaction profile. By measuring the energy of the transition state (relative
709 to the starting material) over a range of reaction coordinate values, it is possible to deduce the
710 structure of species that lie close in energy to the transition state (the structure with typically the
711 highest energy in the reaction coordinate). By then applying a transition-state optimisation to ensure
712 a single, imaginary vibrational-frequency contibution, a more accurate description of the transition
713 state and the activation energy can be determined. More advanced methodologies can perform
714 transition-state optimisation using only the coordinates of the reactant and product species, however
715 the better the initial guess, the more realistic the outcome.[102]

716   More recently, cluster models have been used to study the catalytic sites (including Brønsted
717 sites, silanol nests and isolated silanols) that are active for the Beckmann rearrangement (Figure
718 14).[103-105] In the case of zeotype materials, cluster models typically invoke a ring of 10 – 12 T-sites,
719 depending on the framework used, and smaller oximes (formaldehyde oxime or acetoxime) to
720 minimise the computational cost.[101,103,106] Using this approach, the activation energy for each
721 mechanistic step of the Beckmann rearrangement was assessed for the different types of acid
722 site.[105]The multi-step model showed that, depending on the active centre, the energetics of the
723 reaction could be modified to such an extent that the rate-determining step (RDS) was altered. In this
724 case, different strength acid sites show variable degrees of interaction with reactive species, causing
725 the energetics of transition states (and hence the RDS) of the Beckmann rearrangement to be modified.
726 This was particularly noticeable for the rearrangement of cyclohexanone oxime in mordenite zeolite,
727 where stronger Brønsted acid sites were more effective at stabilising the transition state for nitrogen-
728 insertion relative to weaker silanol species.[105] As a result, at a Brønsted site the activation energy
729 for nitrogen-insertion step fell below that of carbiminium ion hydrolysis, whereas at a silanol site
730 nitrogen-insertion remained the largest activation barrier.[105] Although insightful, this type of 'bare
731 cluster' model still shows discord with experimental activation energies. The methodology has,

732   however, proven well-suited to the study of homogeneous catalysts, where there is little need for
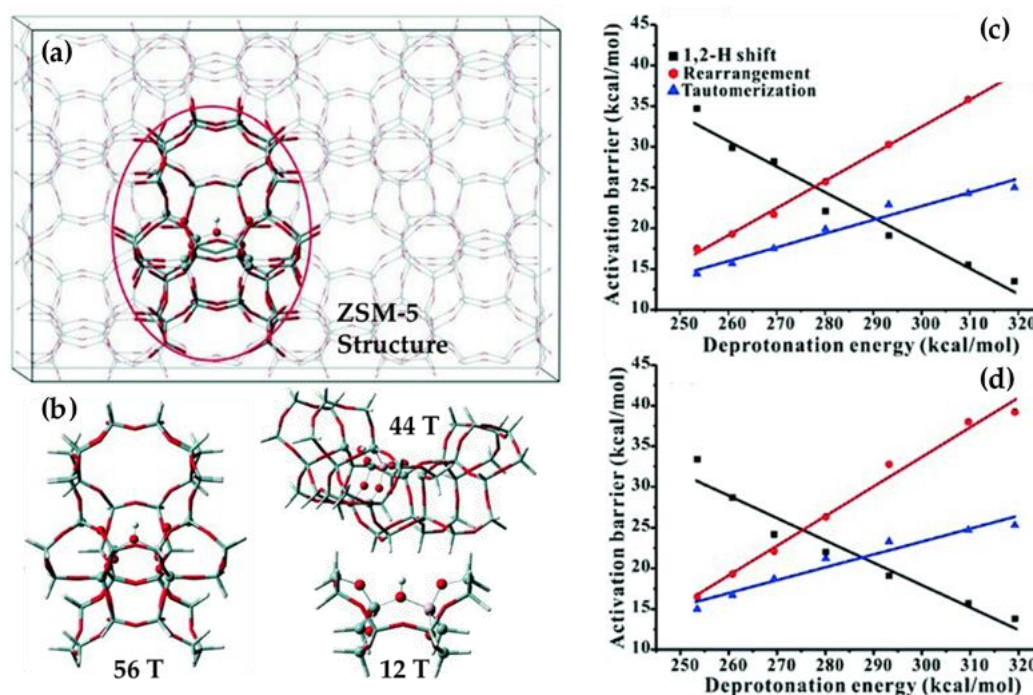733   periodicity or confinement.

737   To account for confinement effects in porous systems, two computational models have been
738   developed. One option is to model a larger cluster (up to 72 T-sites) or a periodic framework, although
739   this is a relatively computationally-demanding approach.[107,108] Alternatively, a combined
740   QM/MM method can be adopted, whereby the active site and oxime are modelled using QM, whilst
741   the influence of the wider framework is accounted for using MM force fields.[106,109] This is known
742   as the 'embedded-cluster' approach. In either case, by including confinement effects it has been
743   shown that the Van der Waals (VdW) interactions between cyclohexanone oxime and zeotype pore
744   walls leads to stabilisation of the transition states. As such, embedded-cluster models have achieved
745   a harmony between theoretical and experimental results.

746   More recently, computational techniques have been used to extrapolate the relationship between
747   acid-site strength and reaction energetics. For weakly-acidic microporous zeotypes (e.g. B-ZSM-5), a
748   higher deprotonation energy (273-319 kcal mol^{-1}) was found to correspond to a well-stabilised
749   transition state for the 1,2-H shift (activation energy 14 kcal mol^{-1}), relative to tautomerisation and
750   rearrangement (25 and 38 kcal mol^{-1}, respectively). However, on increasing the acid site strength (i.e.
751   deprotonation energy < 273 kcal mol^{-1}) transition-state of the 1,2-H shift is destabilised, whilst that of
752   the tautomerisation and rearrangement steps is stabilised (35, 15 and 18 kcal mol^{-1}, respectively). A
753   linear correlation between acid-site strength and activation energy indicated that a system of
754   moderate acidity (i.e. a deprotonation energy of 275 – 285 kcal mol^{-1}) would exhibit the net lowest
755   activation energy for the process.[107] However, both experiment and computation have shown that
756   the same phenomenon is not active in the weakly-acidic, mesoporous MCM-41 system, where the
757   larger pores (and hence weaker VdWs interactions) are unable to stabilise the transition states to the

758   same extent.[107] Computational modelling has also proven instrumental in locating the active site
759   of the industrial MFI catalyst; a controverted topic in the Beckmann rearrangement literature. Based
760   on empirical studies, it was proposed that small pore apertures of the MFI framework (~ 5.4 Å) hinder
761   the migration of caprolactam through the framework, confining the Beckmann rearrangement of
762   cyclohexanone oxime to external sites on the catalyst surface. Nonetheless, adsorption studies also
763   showed that both cyclohexanone oxime and caprolactam could be internalised by Silicalite-1,
764   suggesting that the rearrangement process could occur at internal acid sites within the micropores.
765   Based on computational arguments, however, it has since been proposed that catalysis occurs at nest
766   silanols, located just inside the pore mouths of the MFI framework.[108] In this study, the energetics
767   of the transition states associated with the 1,2-H shift, rearrangement, and tautomerisation steps at
768   598 K were compared for a surface and inside a pore. It was shown that, whilst VdW interactions
769   offset the enthalpic contributions associated with confining cyclohexanone oxime within the MFI
770   pore, a high entropic barrier favoured reaction at the pore-mouths or external surfaces.[108]

771   Arguably, it is the integration of theory with characterisation that has been authoritative in
772   catalyst studies, as demonstrated by solid-state NMR studies.[110] When boron-doped zeolite was
773   combined with isotopically-labelled ^{15}N-cyclohexanone oxime, a host of signals were produced in
774   both the ^{11}B and ^{15}N MAS NMR spectra. However, using DFT modelling it was possible to calculate
775   the chemical shift of various intermediate and bound structures, and hence assign the NMR
776   signals.[111] In this way, it was possible to elucidate the mechanism of the Beckmann rearrangement
777   in B-ZSM-5 and B-Zeolite-β. Similar protocols have also been employed in the wider remit of solid-
778   acid catalysis, illustrating, for example, how the ^{1}H NMR chemical shift of a bound pyrrole molecule
779   can be used to determine the acid strength of zeolites.[112]

780   Theoretical studies have provided invaluable insight into catalyst mechanism and directed
781   material design. Nonetheless, in a comprehensive understanding of catalyst operation, many areas
782   are still available for novel *ab inito* studies. Molecular mechanics simulation, for example, has much
783   to offer, particularly with the emergence of hierarchical species. Such simulations could be used to
784   model the diffusion pathways of reagents and products under realistic operating conditions in order
785   to assess how pore structure affects mass transport. As *in operando* and *in situ* techniques become
786   more mainstream, the potential for synchronising these with theoretical studies offers further
787   opportunities. *Ergo*, it will be important to develop more holistic computational models that can
788   extend beyond the fundamental substrate-framework interactions to incorporate other important
789   experimental parameters, thus evolving model structures into realistic systems.

790   **5. Conclusions**

791   As the chemical industry strives towards more sustainable operations, large-scale production of
792   ε-caprolactam is being revolutionised by the development of highly-selective solid-acid catalysts.
793   These advancements have been underpinned by advancing characterisation techniques and
794   computational methods that seek to understand catalyst activity and mechanism through the
795   influence of zeolite structure and interactions. Studies of the Beckmann rearrangement process in
796   nanoporous materials has demonstrated the power of allying theoretical and empirical studies. The
797   active-site design that has been achieved through the combination of techniques described in this
798   venture serves as a valuable blueprint to the catalysis community as a whole.

799

800   **Reference**

801   1.   Misra, M.; Pandey, J.K.; Mohanty, A. *Biocomposites: Design and mechanical performance*. Elsevier Science:
802   Cambridge, 2015.

803   2.   Nylon 6 & 66 market size worth $41.13 billion by 2025 | cagr: 6.1%.
804   http://www.grandviewresearch.com/press-release/global-nylon-6-66-market (17/11/2017),

805   3.   Raja, R. Designed nanoporous solids for the green production of vitamins, fine chemicals and
806   renewable nylons. *Top Catal* **2009**, *52*, 322-332.

807   4.   Lancaster, M. *Green chemistry: An introductory text*. Royal Society of Chemistry: Cambridge, 2010.

808   5.   Mokaya, R.; Poliakoff, M. Chemistry: A cleaner way to nylon? *Nature* **2005**, *437*, 1243-1244.

809   6.   Baoning Zong, B.S., Shibiao Cheng,Xuhong Mu,Keyong Yang,Junqi Zhao,Xiaoxin Zhang,Wei Wu.
810   Green production technology of the monomer of nylon-6: Caprolactam. *Engineering* **2017**, *3*, 379-384.

811   7.   Polyamide 6 (pa6) - global trends, estimates and forecasts, 2012-2018.
812   http://www.prnewswire.com/news-releases/polyamide-6-pa6---global-trends-estimates-and-forecasts-
813   2012-2018-300092015.html (20/06/2017),

814   8.   Ritz, J.; Fuchs, H.; Kieczka, H.; Mora, W.C. *Ullmann's encyclopedia of industrial chemistry*. 6 ed.; Wiley-
815   VCH: Weinheim, 2002.

816   9.   Sheldon, R.A.; Downing, R.S. Heterogeneous catalytic transformations for environmentally friendly
817   production. *Applied Catalysis A: General* **1999**, *189*, 163-183.

818   10. Harris, K.D.M.; Edwards, P.P. *Turning points in solid-state, materials and surface state: A book in
819   celebration of the life and work of sir john meurig thomas*. The Royal Society of Chemistry: Cambridge,
820   2008.

821   11. Lasier, W.A.; Rigby, G.W. Catalytic process for the production of caprolactam, amino-capronitrile and
822   hexamethylene diamine. US2234566 A, 1941.

823   12. Miletto, I.; Paul, G.; Chapman, S.; Gatti, G.; Marchese, L.; Raja, R.; Gianotti, E. Mesoporous silica
824   scaffolds as precursors to drive the formation of hierarchical sapo-34 with tunable acid properties.
825   *Chemistry - A European Journal* **2017**, *23*, 9952-9961.

826   13. Chang, A.; Hsiao, H.-M.; Chen, T.-H.; Chu, M.-W.; Yang, C.-M. Hierarchical silicalite-1 octahedra
827   comprising highly-branched orthogonally-stacked nanoplates as efficient catalysts for vapor-phase
828   beckmann rearrangement. *Chemical Communications* **2016**, *52*, 11939-11942.

829   14. Maronna, M.M.; Kruissink, E.C.; Parton, R.F.; Tinge, J.T.; Soulimani, F.; Weckhuysen, B.M.;
830   Hoelderich, W.F. Nbox/sio2 in the gas-phase beckmann rearrangement of cyclohexanone oxime to ε-
831   caprolactam: Influence of calcination temperature, niobia loading and silylation post-treatment.
832   *Applied Catalysis B: Environmental* **2016**, *185*, 272-280.

833   15. Bordoloi, A.; Halligudi, S.B. Catalytic properties of wox/sba-15 for vapor-phase beckmann
834   rearrangement of cyclohexanone oxime. *Applied Catalysis A: General* **2010**, *379*, 141-147.

835   16. Kumar, R.; Shah, S.; Bahadur, J.; Melnichenko, Y.B.; Sen, D.; Mazumder, S.; Vinod, C.P.; Chowdhury,
836   B. Highly stable in-sba-15 catalyst for vapor phase beckmann rearrangement reaction. *Microporous and
837   Mesoporous Materials* **2016**, *234*, 293-302.

838   17. Kumar, R.; Enjamuri, N.; Pandey, J.K.; Sen, D.; Mazumder, S.; Bhaumik, A.; Chowdhury, B. Bismuth
839   supported sba-15 catalyst for vapour phase beckmann rearrangement reaction of cyclohexanone
840   oxime to ε-caprolactam. *Applied Catalysis A: General* **2015**, *497*, 51-57.

841   18.   Vaschetto, E.G.; Casuscelli, S.G.; Eimer, G.A. Improvements in the beckmann rearrangement process
842   by using highly selective mesoporous catalysts. *Microporous and Mesoporous Materials* **2016**, *221*, 175-
843   181.
844   19.   Zhang, D.; Wang, R.; Yang, X. Beckmann rearrangement of cyclohexanone oxime over al-mcm-41 and
845   p modified al-mcm-41 molecular sieves. *Catalysis Communications* **2011**, *12*, 399-402.
846   20.   Potter, M.E.; Sun, D.; Raja, R. The curious effects of integrating bimetallic active centres within
847   nanoporous architectures for acid-catalysed transformations. *Catalysis Science & Technology* **2016**, *6*,
848   2616-2622.
849   21.   Deng, Y.-Q.; Yin, S.-F.; Au, C.-T. Preparation of nanosized silicalite-1 and its application in vapor-
850   phase beckmann rearrangement of cyclohexanone oxime. *Industrial & Engineering Chemistry Research*
851   **2012**, *51*, 9492-9499.
852   22.   Kim, J.; Park, W.; Ryoo, R. Surfactant-directed zeolite nanosheets: A high-performance catalyst for
853   gas-phase beckmann rearrangement. *ACS Catalysis* **2011**, *1*, 337-341.
854   23.   Zhang, Y.; Wang, Y.; Bu, Y. Vapor phase beckmann rearrangement of cyclohexanone oxime on hβ-
855   zeolites treated by ammonia. *Microporous and Mesoporous Materials* **2008**, *107*, 247-251.
856   24.   Ichihashi, H.; Sato, H. The development of new heterogeneous catalytic processes for the production
857   of ε-caprolactam. *Applied Catalysis A: General* **2001**, *221*, 359-366.
858   25.   Dahlhoff, G.; Niederer, J.P.M.; Hoelderich, W.F. ε-caprolactam: New by-product free synthesis routes.
859   *Catalysis Reviews* **2001**, *43*, 381-441.
860   26.   Yoshitaka, I.; Hiroshi, I.; Yasumoto, S.; Masaru, K.; Hiroshi, S. Development and industrialization of
861   the vapor-phase beckmann rearrangement process. *Bulletin of the Chemical Society of Japan* **2007**, *80*,
862   1280-1287.
863   27.   Kumar, R.; Chowdhury, B. Comprehensive study for vapor phase beckmann rearrangement reaction
864   over zeolite systems. *Industrial & Engineering Chemistry Research* **2014**, *53*, 16587-16599.
865   28.   Bellussi, G.; Millini, R.; Pollesel, P.; Perego, C. Zeolite science and technology at eni. *New Journal of
866   Chemistry* **2016**, *40*, 4061-4077.
867   29.   Pavel, C.C.; Palkovits, R.; Schüth, F.; Schmidt, W. The benefit of mesopores in ets-10 on the vapor-
868   phase beckmann rearrangement of cyclohexanone oxime. *Journal of Catalysis* **2008**, *254*, 84-90.
869   30.   Cesana, A.; Palmery, S.; Buzzoni, R.; Spanò, G.; Rivetti, F.; Carnelli, L. Silicalite-1 deactivation in
870   vapour phase beckmann rearrangement of cyclohexanone oxime to caprolactam. *Catalysis Today* **2010**,
871   *154*, 264-270.
872   31.   Ge, C.; Li, Z.; Chen, G.; Qin, Z.; Li, X.; Dou, T.; Dong, M.; Chen, J.; Wang, J.; Fan, W. Kinetic study of
873   vapor-phase beckmann rearrangement of cyclohexanone oxime over silicalite-1. *Chemical Engineering
874   Science* **2016**, *153*, 246-254.
875   32.   Chapman, S.; Raja, R. Expanding beyond the micropore: Catalysis with hierarchical architectures.
876   *Advanced Science Letters* **2017**, *23*, 5995-5997.
877   33.   Holm, M.S.; Taarning, E.; Egeblad, K.; Christensen, C.H. Catalysis with hierarchical zeolites. *Catalysis
878   Today* **2011**, *168*, 3-16.
879   34.   Yin, C.; Ni, R.; Bao, X.; Chen, Y. Synthesis of hierarchical porous silicalite-1 and its catalytic
880   performance in beckmann rearrangement. *Microporous and Mesoporous Materials* **2015**, *202*, 133-137.
881   35.   Hartmann, M.; Schwieger, W. Hierarchically-structured porous materials: From basic understanding
882   to applications. *Chemical Society Reviews* **2016**, *45*, 3311-3312.

883   36.   Newland, S.H.; Sinkler, W.; Mezza, T.; Bare, S.R.; Carravetta, M.; Haies, I.M.; Levy, A.; Keenan, S.;
884   Raja, R. Expanding beyond the micropore: Active-site engineering in hierarchical architectures for
885   beckmann rearrangement. *ACS Catalysis* **2015**, *5*, 6587-6593.

886   37.   Palkovits, R.; Schmidt, W.; Ilhan, Y.; Erdem-Şenatalar, A.; Schüth, F. Crosslinked ts-1 as stable catalyst
887   for the beckmann rearrangement of cyclohexanone oxime. *Microporous and Mesoporous Materials* **2009**,
888   *117*, 228-232.

889   38.   Wei, H.; Zhang, N.; Zhao, T.; Liu, Y.; Wen, Y.; Wang, X.; Li, B. Controlling the microstructure of mfi
890   zeolites with mg(oh)2 nanocrystals to improve their catalytic performances. *RSC Advances* **2015**, *5*,
891   3642-3647.

892   39.   Meng, F.; Wang, Y.; Wang, L.; Yang, R.; Zhang, T. Influence of br− and na+ in synthesis of silicalite-1
893   on catalytic performance in vapor phase beckmann rearrangement of cyclohexanone oxime. *Journal of*
894   *Molecular Catalysis A: Chemical* **2011**, *335*, 105-111.

895   40.   Wei, H.; Zhao, T.; Liu, Y.; Li, G.; Wang, X.; Li, B. Synthesis of ts-1 submicrocrystals from inorganic
896   reactants by a seed method for the vapor beckmann rearrangement of cyclohexanone oxime. *RSC*
897   *Advances* **2013**, *3*, 20811-20815.

898   41.   Botella, P.; Corma, A.; Iborra, S.; Montón, R.; Rodríguez, I.; Costa, V. Nanosized and delayered
899   zeolitic materials for the liquid-phase beckmann rearrangement of cyclododecanone oxime. *Journal of*
900   *Catalysis* **2007**, *250*, 161-170.

901   42.   Raja, R.; Potter, M.E.; Newland, S.H. Predictive design of engineered multifunctional solid catalysts.
902   *Chemical Communications* **2014**, *50*, 5940-5957.

903   43.   Ngamcharussrivichai, C.; Wu, P.; Tatsumi, T. Active and selective catalyst for liquid phase beckmann
904   rearrangement of cyclohexanone oxime. *Journal of Catalysis* **2005**, *235*, 139-149.

905   44.   Camblor, M.A.; Corma, A.; García, H.; Semmer-Herlédan, V.; Valencia, S. Active sites for the liquid-
906   phase beckmann rearrangement of cyclohexanone, acetophenone and cyclododecanone oximes,
907   catalyzed by beta zeolites. *Journal of Catalysis* **1998**, *177*, 267-272.

908   45.   Thomas, J.M.; Raja, R.; Lewis, D.W. Single-site heterogeneous catalysts. *Angewandte Chemie*
909   *International Edition* **2005**, *44*, 6456-6482.

910   46.   Cheetham, A.K.; Férey, G.; Loiseau, T. Open-framework inorganic materials. *Angewandte Chemie*
911   *International Edition* **1999**, *38*, 3268-3292.

912   47.   Potter, M.E.; Sun, D.; Gianotti, E.; Manzoli, M.; Raja, R. Investigating site-specific interactions and
913   probing their role in modifying the acid-strength in framework architectures. *Physical Chemistry*
914   *Chemical Physics* **2013**, *15*, 13288-13295.

915   48.   Gianotti, E.; Manzoli, M.; Potter, M.E.; Shetti, V.N.; Sun, D.; Paterson, J.; Mezza, T.M.; Levy, A.; Raja,
916   R. Rationalising the role of solid-acid sites in the design of versatile single-site heterogeneous catalysts
917   for targeted acid-catalysed transformations. *Chemical Science* **2014**, *5*, 1810-1819.

918   49.   Vaschetto, E.G.; Monti, G.A.; Herrero, E.R.; Casuscelli, S.G.; Eimer, G.A. Influence of the synthesis
919   conditions on the physicochemical properties and acidity of al-mcm-41 as catalysts for the
920   cyclohexanone oxime rearrangement. *Applied Catalysis A: General* **2013**, *453*, 391-402.

921   50.   Vaschetto, E.G.; Pecchi, G.A.; Casuscelli, S.G.; Eimer, G.A. Nature of the active sites in al-mcm-41
922   nano-structured catalysts for the selective rearrangement of cyclohexanone oxime toward ε-
923   caprolactam. *Microporous and Mesoporous Materials* **2014**, *200*, 110-116.
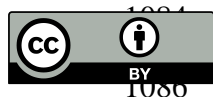
924 51. Ngamcharussrivichai, C.; Wu, P.; Tatsumi, T. Liquid-phase beckmann rearrangement of
925 cyclohexanone oxime over mesoporous molecular sieve catalysts. *Journal of Catalysis* **2004**, *227*, 448-
926 458.

927 52. Zhang, D.; Wang, R.; Wang, L.; Yang, X. Coking and deactivation of boron modified al-mcm-41 for
928 vapor-phase beckmann rearrangement reaction. *Journal of Molecular Catalysis A: Chemical* **2013**, *366*,
929 179-185.

930 53. Wang, X.; Chen, C.-C.; Chen, S.-Y.; Mou, Y.; Cheng, S. Arenesulfonic acid functionalized mesoporous
931 silica as a novel acid catalyst for the liquid phase beckmann rearrangement of cyclohexanone oxime to
932 ε-caprolactam. *Applied Catalysis A: General* **2005**, *281*, 47-54.

933 54. Anilkumar, M.; Hoelderich, W.F. Gas phase beckmann rearrangement of cyclohexanone oxime to ε-
934 caprolactam over mesoporous, microporous and amorphous nb2O5/silica catalysts: A comparative
935 study. *Catalysis Today* **2012**, *198*, 289-299.

936 55. Maronna, M.M.; Kruissink, E.C.; Tinge, J.T.; Agar, D.W.; Hoelderich, W.F. Kinetic study on gas-phase
937 beckmann rearrangement of cyclohexanone oxime to ε-caprolactam over a silica-supported niobia
938 catalyst. *Industrial & Engineering Chemistry Research* **2016**, *55*, 1202-1214.

939 56. Anilkumar, M.; Hoelderich, W.F. New non-zeolitic nb-based catalysts for the gas-phase beckmann
940 rearrangement of cyclohexanone oxime to caprolactam. *Journal of Catalysis* **2012**, *293*, 76-84.

941 57. Mandal, S.; Santra, C.; Kumar, R.; Pramanik, M.; Rahman, S.; Bhaumik, A.; Maity, S.; Sen, D.;
942 Chowdhury, B. Niobium doped hexagonal mesoporous silica (HMS-X) catalyst for vapor phase
943 beckmann rearrangement reaction. *RSC Advances* **2014**, *4*, 845-854.

944 58. Maronna, M.M.; Kruissink, E.C.; Parton, R.F.; Soulimani, F.; Weckhuysen, B.M.; Hoelderich, W.F.
945 Spectroscopic study on the active site of a sio2 supported niobia catalyst used for the gas-phase
946 beckmann rearrangement of cyclohexanone oxime to ?-caprolactam. *Physical Chemistry Chemical*
947 *Physics* **2016**, *18*, 22636-22646.

948 59. Anilkumar, M.; Hoelderich, W.F. A one step synthesis ofcaprolactam out of cyclohexanone by
949 combinded ammoximation and beckmann rearrangement over nb-mcm-41 catalysts. *Applied Catalysis*
950 *B: Environmental* **2015**, *165*, 87-93.

951 60. Levy, A.B.; Raja, R.; Potter, M.E. Gas and liquid phase catalytic beckmann rearrangement of oximes to
952 produce lactams. US8772476 B2, 2014.

953 61. Jacobs, P.A.; Von Ballmoos, R. Framework hydroxyl groups of h-zsm-5 zeolites. *The Journal of Physical*
954 *Chemistry* **1982**, *86*, 3050-3052.

955 62. Jacobs, P.A.; Mortier, W.J. An attempt to rationalize stretching frequencies of lattice hydroxyl groups
956 in hydrogen-zeolites. *Zeolites* **1982**, *2*, 226-230.

957 63. Datka, J.; Geerlings, P.; Mortier, W.; Jacobs, P. Influence of the overall composition on zeolite
958 properties. 1. The framework: An infrared spectroscopic and quantum chemical study. *The Journal of*
959 *Physical Chemistry* **1985**, *89*, 3483-3488.

960 64. Topsøe, N.-Y.; Pedersen, K.; Derouane, E.G. Infrared and temperature-programmed desorption study
961 of the acidic properties of zsm-5-type zeolites. *Journal of Catalysis* **1981**, *70*, 41-52.

962 65. Ichihashi, H.; Ishida, M.; Shiga, A.; Kitamura, M.; Suzuki, T.; Suenobu, K.; Sugita, K. The catalysis of
963 vapor-phase beckmann rearrangement for the production of ε-caprolactam. *Catalysis Surveys from Asia*
964 **2003**, *7*, 261-270.

965 66. Heitmann, G.P.; Dahlhoff, G.; Hölderich, W.F. Catalytically active sites for the beckmann
966 rearrangement of cyclohexanone oxime to ε-caprolactam. *Journal of Catalysis* **1999**, *186*, 12-19.

967   67.   Ichihashi, H.; Kitamura, M. Some aspects of the vapor phase beckmann rearrangement for the
968   production of ε-caprolactam over high silica mfi zeolites. *Catalysis Today* **2002**, *73*, 23-28.

969   68.   Hölderich, W.F.; Röseler, J.; Heitmann, G.; Liebens, A.T. The use of zeolites in the synthesis of fine
970   and intermediate chemicals. *Catalysis Today* **1997**, *37*, 353-366.

971   69.   Ichihashi, H.; Kitamura, M.; Tojima, H. Process for producing epsilon-caprolactam and activating
972   solid catalysts therefor. Google Patents: 1998.

973   70.   Sato, H.; Hirose, K.; Kitamura, M.; Nakamura, Y. A vapor phase beckmann rearrangement over high-
974   silicious zsm-5. In *Studies in surface science and catalysis*, Jacobs, P.A.; van Santen, R.A., Eds. Elsevier:
975   1989; Vol. 49, pp 1213-1222.

976   71.   Lercher, J.A.; Gründling, C.; Eder-Mirth, G. Infrared studies of the surface acidity of oxides and
977   zeolites using adsorbed probe molecules. *Catalysis Today* **1996**, *27*, 353-376.

978   72.   Chon, H.; Woo, S.I.; Park, S.E. *Recent advances and new horizons in zeolite science and technology*. Elsevier
979   Science: Amsterdam, 1996.

980   73.   Flego, C.; Dalloro, L. Beckmann rearrangement of cyclohexanone oxime over silicalite-1: An ft-ir
981   spectroscopic study. *Microporous and Mesoporous Materials* **2003**, *60*, 263-271.

982   74.   Singh, P.S.; Bandyopadhyay, R.; Hegde, S.G.; Rao, B.S. Vapour phase beckmann rearrangement of
983   cyclohexanone oxime over sapo-11 molecular sieve. *Applied Catalysis A: General* **1996**, *136*, 249-263.

984   75.   Levy, A.B.; Raja, R.; Newland, S.H.; Keenan, S.R.; Bare, S.R. Hierarchical aluminophosphates as
985   catalysts for the beckmann rearrangement. US 20160167030 A1, 2016.

986   76.   Viswanathan, B.; Sivasanker, S.; Ramaswamy, A.V. *Catalysis: Principles and applications*. Narosa
987   Publishing House: New Delhi, 2002.

988   77.   Sierra de Saldarriaga, L.; Saldarriaga, C.; Davis, M.E. Investigations into the nature of a
989   silicoaluminophosphate with the faujasite structure. *Journal of the American Chemical Society* **1987**, *109*,
990   2686-2691.

991   78.   Potter, M.E.; O'Malley, A.J.; Chapman, S.; Kezina, J.; Newland, S.H.; Silverwood, I.P.; Mukhopadhyay,
992   S.; Carravetta, M.; Mezza, T.M.; Parker, S.F., *et al.* Understanding the role of molecular diffusion and
993   catalytic selectivity in liquid-phase beckmann rearrangement. *ACS Catalysis* **2017**, *7*, 2926-2934.

994   79.   Potter, M.E.; Chapman, S.; O'Malley, A.J.; Levy, A.; Carravetta, M.; Mezza, T.M.; Parker, S.F.; Raja, R.
995   Understanding the role of designed solid acid sites in the low-temperature production of ε-
996   caprolactam. *ChemCatChem* **2017**, *9*, 1897-1900.

997   80.   Jones, M.O.; Taylor, A.D.; Parker, S.F. Neutron scattering studies of catalyst systems at the isis
998   neutron spallation source. *Appl Petrochem Res* **2012**, *2*, 97-104.

999   81.   Blasco, T. Insights into reaction mechanisms in heterogeneous catalysis revealed by in situ nmr
1000   spectroscopy. *Chemical Society Reviews* **2010**, *39*, 4685-4702.

1001   82.   Zhang, W.; Xu, S.; Han, X.; Bao, X. In situ solid-state nmr for heterogeneous catalysis: A joint
1002   experimental and theoretical approach. *Chemical Society Reviews* **2012**, *41*, 192-210.

1003   83.   Zheng, A.; Li, S.; Liu, S.-B.; Deng, F. Acidic properties and structure–activity correlations of solid acid
1004   catalysts revealed by solid-state nmr spectroscopy. *Accounts of Chemical Research* **2016**, *49*, 655-663.

1005   84.   Anilkumar, M.; Hölderich, W.F. Highly active and selective nb modified mcm-41 catalysts for
1006   beckmann rearrangement of cyclohexanone oxime to ε-caprolactam. *Journal of Catalysis* **2008**, *260*, 17-
1007   29.

1008   85.   Korányi, T.I.; Nagy, J.B. Distribution of aluminum and boron in the periodical building units of
1009   boron-containing β zeolites. *The Journal of Physical Chemistry B* **2006**, *110*, 14728-14735.

86.　Alzeer, M.I.M.; MacKenzie, K.J.D.; Keyzers, R.A. Porous aluminosilicate inorganic polymers (geopolymers): A new class of environmentally benign heterogeneous solid acid catalysts. *Applied Catalysis A: General* **2016**, *524*, 173-181.

87.　Conesa, T.D.; Mokaya, R.; Yang, Z.; Luque, R.; Campelo, J.M.; Romero, A.A. Novel mesoporous silicoaluminophosphates as highly active and selective materials in the beckmann rearrangement of cyclohexanone and cyclododecanone oximes. *Journal of Catalysis* **2007**, *252*, 1-10.

88.　Reddy Marthala, V.R.; Wang, W.; Jiao, J.; Jiang, Y.; Huang, J.; Hunger, M. Effect of probe molecules with different proton affinities on the coordination of boron atoms in dehydrated zeolite h-[b]zsm-5. *Microporous and Mesoporous Materials* **2007**, *99*, 91-97.

89.　Garcia Vargas, N.; Stevenson, S.; Shantz, D.F. Simultaneous isomorphous incorporation of boron and germanium in mfi zeolites. *Microporous and Mesoporous Materials* **2013**, *170*, 131-140.

90.　Springuel-Huet, M.A.; Guenneau, F.; Gédéon, A.; Corma, A. Probing xe exchange in delaminated zeolites by hyperpolarized 129xe nmr. *The Journal of Physical Chemistry C* **2007**, *111*, 5694-5700.

91.　Liu, Y.; Zhang, W.; Liu, Z.; Xu, S.; Wang, Y.; Xie, Z.; Han, X.; Bao, X. Direct observation of the mesopores in zsm-5 zeolites with hierarchical porous structures by laser-hyperpolarized 129xe nmr. *The Journal of Physical Chemistry C* **2008**, *112*, 15375-15381.

92.　Bonelli, B.; Forni, L.; Aloise, A.; Nagy, J.B.; Fornasari, G.; Garrone, E.; Gedeon, A.; Giordano, G.; Trifirò, F. Beckmann rearrangement reaction: About the role of defect groups in high silica zeolite catalysts. *Microporous and Mesoporous Materials* **2007**, *101*, 153-160.

93.　Reddy Marthala, V.R.; Frey, J.; Hunger, M. Accessibility and interaction of surface oh groups in microporous and mesoporous catalysts applied for vapor-phase beckmann rearrangement of oximes. *Catalysis Letters* **2010**, *135*, 91-97.

94.　Fernández, A.B.; Boronat, M.; Blasco, T.; Corma, A. Establishing a molecular mechanism for the beckmann rearrangement of oximes over microporous molecular sieves. *Angewandte Chemie International Edition* **2005**, *44*, 2370-2373.

95.　Huo, H.; Peng, L.; Gan, Z.; Grey, C.P. Solid-state mas nmr studies of brønsted acid sites in zeolite h-mordenite. *Journal of the American Chemical Society* **2012**, *134*, 9708-9720.

96.　O'Neil Parker, W. Chemical transformations on a weakly acidic catalyst studied by 15n nmr: Butanone oxime on silicalite-1. *Magnetic Resonance in Chemistry* **1999**, *37*, 433-436.

97.　Reddy Marthala, V.R.; Jiang, Y.; Huang, J.; Wang, W.; Gläser, R.; Hunger, M. Beckmann rearrangement of 15n-cyclohexanone oxime on zeolites silicalite-1, h-zsm-5, and h-[b]zsm-5 studied by solid-state nmr spectroscopy. *Journal of the American Chemical Society* **2006**, *128*, 14812-14813.

98.　Reddy Marthala, V.R.; Rabl, S.; Huang, J.; Rezai, S.A.S.; Thomas, B.; Hunger, M. In situ solid-state nmr investigations of the vapor-phase beckmann rearrangement of 15n-cyclohexanone oxime on mfi-type zeolites and mesoporous sba-15 materials in the absence and presence of the additive 13c-methanol. *Journal of Catalysis* **2008**, *257*, 134-141.

99.　Ronchin, L.; Bortoluzzi, M.; Vavasori, A. A dft study on secondary reaction pathways in the acid-catalysed beckmann rearrangement of cyclohexanone oxime in aprotic solvent. *Journal of Molecular Structure: THEOCHEM* **2008**, *858*, 46-51.

100.　Takahashi, H.; Tanabe, K.; Aketa, M.; Kishi, R.; Furukawa, S.-i.; Nakano, M. Novel quantum mechanical/molecular mechanical method combined with the theory of energy representation: Free energy calculation for the beckmann rearrangement promoted by proton transfers in the supercritical water. *The Journal of Chemical Physics* **2007**, *126*, 084508.

1053 101. Adamo, C.; Jacquemin, D. The calculations of excited-state properties with time-dependent density
1054 functional theory. *Chemical Society Reviews* **2013**, *42*, 845-856.

1055 102. Sirijaraensre, J.; Limtrakul, J. Vapor-phase beckmann rearrangement of oxime molecules over h-
1056 faujasite zeolite. *ChemPhysChem* **2006**, *7*, 2424-2432.

1057 103. Ishida, M.; Suzuki, T.; Ichihashi, H.; Shiga, A. Theoretical study on vapour phase beckmann
1058 rearrangement of cyclohexanone oxime over a high silica mfi zeolite. *Catalysis Today* **2003**, *87*, 187-194.

1059 104. Bucko, T.; Hafner, J.; Benco, L. Active sites for the vapor phase beckmann rearrangement over
1060 mordenite: An ab initio study. *The Journal of Physical Chemistry A* **2004**, *108*, 11388-11397.

1061 105. Sirijaraensre, J.; Truong, T.N.; Limtrakul, J. Density functional study of the mechanism of the
1062 beckmann rearrangement catalyzed by h-zsm-5: A cluster and embedded cluster study. *The Journal of*
1063 *Physical Chemistry B* **2005**, *109*, 12099-12106.

1064 106. Chu, Y.; Ji, P.; Yi, X.; Li, S.; Wu, P.; Zheng, A.; Deng, F. Strong or weak acid, which is more efficient for
1065 beckmann rearrangement reaction over solid acid catalysts? *Catalysis Science & Technology* **2015**, *5*,
1066 3675-3681.

1067 107. Chu, Y.; Li, G.; Huang, L.; Yi, X.; Xia, H.; Zheng, A.; Deng, F. External or internal surface of h-zsm-5
1068 zeolite, which is more effective for the beckmann rearrangement reaction? *Catalysis Science &*
1069 *Technology* **2017**, *7*, 2512-2523.

1070 108. Sirijaraensre, J.; Limtrakul, J. Effect of the acidic strength on the vapor phase beckmann
1071 rearrangement of cyclohexanone oxime over the mfi zeolite: An embedded oniom study. *Physical*
1072 *Chemistry Chemical Physics* **2009**, *11*, 578-585.

1073 109. Lezcano-González, I.; Boronat, M.; Blasco, T. Investigation on the beckmann rearrangement reaction
1074 catalyzed by porous solids: Mas nmr and theoretical calculations. *Solid State Nuclear Magnetic*
1075 *Resonance* **2009**, *35*, 120-129.

1076 110. Lezcano-Gonzalez, I.; Vidal-Moya, A.; Boronat, M.; Blasco, T.; Corma, A. Modelling active sites for the
1077 beckmann rearrangement reaction in boron-containing zeolites and their interaction with probe
1078 molecules. *Physical Chemistry Chemical Physics* **2010**, *12*, 6396-6403.

1079 111. Yi, X.; Li, G.; Huang, L.; Chu, Y.; Liu, Z.; Xia, H.; Zheng, A.; Deng, F. An nmr scale for measuring the
1080 base strength of solid catalysts with pyrrole probe: A combined solid-state nmr experiment and
1081 theoretical calculation study. *The Journal of Physical Chemistry C* **2017**, *121*, 3887-3895.

1087